Structure of forward pp and $p\bar{p}$ elastic amplitudes at low energies

E. Ferreira,[1,*] A. K. Kohara,[1] and J. Sesma[2]

[1]*Instituto de Física, Universidade Federal do Rio de Janeiro, C.P. 68528, Rio de Janeiro 21945-970, RJ, Brazil*
[2]*Departamento de Física Teórica, Facultad de Ciencias, 50009 Zaragoza, Spain*

Exact analytical forms of solutions for dispersion relations for amplitudes and dispersion relations for slopes are applied in the analysis of pp and $p\bar{p}$ scattering data in the forward range at energies below $\sqrt{s} \approx 30$ GeV. As inputs for the energy dependence of the imaginary part, use is made of analytic form for the total cross sections and for parameters of the t dependence of the imaginary parts, with exponential and linear factors. A structure for the t dependence of the real amplitude is written, with slopes B_R and a linear factor $\rho - \mu_R t$ that allows compatibility of the data with the predictions from dispersion relations for the derivatives of the real amplitude at the origin. A very precise description is made of all $d\sigma/dt$ data, with regular energy dependence of all quantities. It is shown that a revision of previous calculations of total cross sections, slopes and ρ parameters in the literature is necessary, and stressed that only determinations based on $d\sigma/dt$ data covering sufficient t range using appropriate forms of amplitudes can be considered as valid.

I. INTRODUCTION

In the scattering theory in quantum mechanics, the elastic differential cross sections are written in terms of a complex amplitude with independent imaginary and real parts, which are functions of two variables s, t (spin effects neglected). In the analysis of observables, besides the nuclear amplitude, account is taken for the contribution from the real Coulomb interaction. This is very basic and obvious, but we show in the present work that this structure is not usually obeyed in the treatments of the pp and $p\bar{p}$ systems, where $d\sigma/dt$ is written without due account for the properties of the amplitudes. We give a treatment of these elastic processes using theoretical constraints and appropriate forms of the input quantities, arriving at realistic amplitudes to connect measurements and theoretical dynamical models.

Determinations of σ, ρ and other parameters of pp and $p\bar{p}$ forward elastic scattering are not direct experimental measurements. Rather, they result from model-dependent analytical limiting procedures, performed with forms assumed for the imaginary and real parts of the complex elastic amplitude. The work done in the laboratory consists in measuring values of the number $\Delta N/\Delta t$ of event rates in intervals $t \to t + \Delta t$. With attention given to fluxes and densities (we are only concerned with unpolarized beams and targets), tables of t distributions in differential cross sections $d\sigma/dt$ are produced. We stress that the identification of the amplitudes and their parameters requires use of proper theoretical framework.

The differential cross section is written as a sum of absolute values

$$\frac{d\sigma}{dt} = \frac{d\sigma_I}{dt} + \frac{d\sigma_R}{dt} = (\hbar c)^2 (|T_I|^2 + |T_R|^2) \qquad (1)$$

and the disentanglement required for the determination of the amplitudes $T_I(s, t)$ and $T_R(s, t)$ is not at all trivial. Help is brought from the interference of nuclear and Coulomb interactions and from dispersion relations connecting real and imaginary parts through general principles of causality and analyticity.

Besides the entanglement to be resolved, we have that production rates are not obtainable directly at the origin $t = 0$, or even very close to it, but rather in sets of points of an interval. The determination of σ, ρ, slopes and other quantities requires extrapolation of data in a $|t|$ range, using analytical expressions, and the results obviously depend on their forms. The mathematical structures of the amplitudes are mounted using parameters that must be found in confront with the observed t distribution in $d\sigma/dt$. Regularity in the behavior of all quantities with the energy is an important consideration to obtain sensible descriptions of the elastic processes. Experiments at different energies must be analyzed globally, since separate fitting procedures may lead to values that are useless as a step for the phenomenology of the area.

---

*Corresponding author.
erasmo@if.ufrj.br

The t range of the data at given energy must be sufficient for representation through assumed analytical forms. In the low energy range, up to $\sqrt{s} \approx 30$ GeV, often these conditions are not satisfied, even suffering insecure normalization in the measurements of $d\sigma/dt$, and compilations of published values for typical parameters result scattered in plots, without coherence and regularity. We propose an investigation of this energy range, with emphasis on the identification of the amplitudes, searching to build a bridge between measurements and mathematical description, necessary to guide models of the dynamics of the processes.

In the interval of $\sqrt{s}$ from 30 to 60 GeV, pp and $p\bar{p}$ from ISR/CERN and Fermilab data cover the large t range with good precision, showing fast increase in σ, a forward peak and a marked dip in $d\sigma/dt$. These measurements led to the establishment of the successful Regge phenomenology [1,2], based on the exchange of particles (Pomerons, Reggeons) in the t channel. Several theoretical models were developed to describe dynamically this region of data in the s and t variables [3].

Above $\sqrt{s} = 60$ GeV, experiments [4] have large energy gaps, passing fast by SPS/CERN, Fermilab and reaching the TeV range of LHC [5]. Ingredients of QCD dynamics enter with less or more detail in the interpretation of these data [6,7]. According to QCD expectations, as the energy increases the response of the gluon density in the hadrons increases and the hadronic interaction becomes determined by the vacuum structure [8,9]. The interpretation of the forward scattering parameters in the LHC experiments at 7, 8 and 13 TeV is not trivial, and ambiguities and possible discrepancies are not clarified [10]. The potential of crucial information [11] in the real part of the forward amplitude at high energies requires that doubts in the analysis of the data be properly solved.

In this paper we analyze forward pp, $p\bar{p}$ data with $\sqrt{s}$ from ≈ 3 to ≈ 30 GeV, using forms for real and imaginary scattering amplitudes restricted to the forward regime and exploring fully the theoretical resources and constraints of dispersion relations treated exactly, in order to extract pure information on the forward quantities, as much as possible independently of peculiar microscopic models. This is the most difficult range of data for the analysis, for both reasons of insufficiency in the data and sophistication of the mathematical solutions of dispersion relations at low energies. Anyhow, we believe that in this sector we can learn about determination of amplitude parameters, and hope that this technical knowledge may be useful in the present difficulties encountered in the analysis of the recent LHC experiments.

We propose a treatment of pp and $p\bar{p}$ forward elastic scattering analyzing all data of differential cross sections that seem qualified (namely covering necessary t range with regularity) for the extraction of the real and imaginary parts of the complex amplitude. We use the simplest and realistically possible analytical forms, treating coherently the Coulomb interference and the Coulomb phase, we use dispersion relations for the amplitudes (DRA) and for their slopes (DRS) [12] with exact solutions for the principal value integrals, obtaining coherent energy dependence of all quantities. DRA and DRS predict algebraic values for the real amplitudes and their derivatives at $t = 0$, and our aim is to have sound proposals for the energy dependence of other parameters in order to reduce flexibility and choices by fittings, and produce a complete coherent description of all data in pp and $p\bar{p}$ unpolarized elastic scattering. To eliminate fluctuations that are not meaningful, we account for normalization uncertainties (systematic errors), investigating a normalization factor in each experiment that adjusts the total cross section to the parametrized prediction. These factors are always very close to 1.

The plots and numbers presented in the Review of Particle Properties [13] of the Particle Data Group for forward scattering parameters in the low energy range, taken from the experimental papers, are scattered and misleading. The results of our work for all data that we analyze are regularly distributed, presented in numbers and very precise plots of $d\sigma/dt$ in Sec. III, showing a way for rationalization of the phenomenological knowledge. However, the proposed solutions are not meant to be conclusive, unique or fully convincing. Alternatives are possible and may be looked for.

In elastic pp and $p\bar{p}$ scattering in the forward direction, the t dependences of the amplitudes are mainly characterized by exponential forms, with slopes B_I and B_R that are essentially independent quantities, essentially not equal to each other: the real and imaginary amplitudes do not run parallel along the t axis. We take special care in the investigation of the behavior of the real part, which has structure deviating from a pure exponential form for t values included in the forward range.

Once the total cross sections for pp and $p\bar{p}$ are parametrized in the energy, the usual dispersion relations for the amplitudes (DRA) determine the real amplitudes at the origin (namely the ρ parameters). Similarly, if the derivatives of the imaginary parts of pp and $p\bar{p}$ at $t = 0$ are given as functions of the energy, the derivatives of the real parts at $t = 0$ are determined by the dispersion relations for slopes (DRS). At low energies it is essential that in both DRA and DRS calculations the exact solutions [14] be used. The dispersion relations for the amplitudes has been effectively used in investigations of the energy dependence of total cross section and ρ parameter in pp and $p\bar{p}$ scattering, being a very important tool of control in the analysis of the data [15].

The imaginary part is positive at $t = 0$ and decreases with an exponential form, which must be multiplied by a proper factor pointing to a zero, so that the well known dip may be created in $d\sigma/dt$. Actually, in our analysis the dip is located outside the examined $|t|$ range, but a linear factor

pointing to a distant zero has influence in the shape of the imaginary amplitude and its extrapolation for $t = 0$ to use the optical theorem. In the real part the effect of the structure (t dependence) beyond the exponential slope is present in the small $|t|$ region, and is essential in DRA and DRS for the determination of the parameter ρ, and here also a factor (linear, in our case) must be introduced.

The solutions for the forward amplitudes can be obtained with high accuracy, minimum freedom of parameters, and with remarkable simplicity and regularity in the energy dependence of all quantities.

Trusting to propose a realistic assumption, we write for the pp or $p\bar{p}$ elastic differential cross sections

$$
\frac{d\sigma}{dt}(pp, p\bar{p})(s, t)
$$
$$
= \pi(\hbar c)^2 \left\{ \left[\frac{\sigma(\rho - \mu_R t)}{4\pi(\hbar c)^2} e^{B_R t/2} + F^C(t) \cos(\alpha\Phi) \right]^2 \right.
$$
$$
\left. + \left[\frac{\sigma(1 - \mu_I t)}{4\pi(\hbar c)^2} e^{B_I t/2} + F^C(t) \sin(\alpha\Phi) \right]^2 \right\}, \quad (2)
$$

where $t \equiv -|t|$ and we call attention for the different values expected for the slopes B_I and B_R of the imaginary and real amplitudes and introduce factors with linear t dependence in each amplitude. This expression is applied for pp and $p\bar{p}$, and the energy dependent quantities $\sigma(s)$, $B_I(s)$, $\mu_I(s)$, $\rho(s)$, $B_R(s)$, $\mu_R(s)$ are specific for each case.

In a given normalization we write for the real and imaginary nuclear (upper label N) amplitudes

$$
T_R^N(s, t) = \frac{1}{4\sqrt{\pi}(\hbar c)^2} \sigma(\rho - \mu_R t) e^{B_R t/2} \quad (3)
$$

and

$$
T_I^N(s, t) = \frac{1}{4\sqrt{\pi}(\hbar c)^2} \sigma(1 - \mu_I t) e^{B_I t/2}. \quad (4)
$$

The optical theorem is implicit in Eq. (4). At $t = 0$, we have the usual definition of the ρ parameter

$$
\rho = \frac{T_R^N(s, t = 0)}{T_I^N(s, t = 0)}, \quad (5)
$$

remarking that the value of ρ obtained by fitting of data in a certain t range depends on the analytical forms (3) and (4) of the amplitudes.

In Eq. (2), α is the fine-structure constant, $\Phi(s, t)$ is the Coulomb phase and $F^C(t)$ is related with the proton form factor

$$
F^C(t) = (-/+)\frac{2\alpha}{|t|} F_{\text{proton}}^2(t), \quad (6)
$$

for the $pp/p\bar{p}$ collisions, where

$$
F_{\text{proton}}(t) = [\Lambda^2/(\Lambda^2 + |t|)]^2, \quad (7)
$$

with $\Lambda^2 = 0.71 \text{ GeV}^2$.

In the present work we follow the usual belief that the phase of the Coulomb-Nuclear interference is based on the superposition of amplitudes in the eikonal formalism [16]. In Appendix A we present the calculation of the Coulomb phase adequate for the amplitudes (3) and (4).

The expressions for the derivatives of the amplitudes are

$$
\frac{d}{dt} T_R^N(s, t)\bigg|_{t=0} = \frac{1}{4\sqrt{\pi}(\hbar c)^2} \sigma \left(\frac{\rho B_R}{2} - \mu_R \right) \quad (8)
$$

and

$$
\frac{d}{dt} T_I^N(s, t)\bigg|_{t=0} = \frac{1}{4\sqrt{\pi}(\hbar c)^2} \sigma \left(\frac{B_I}{2} - \mu_I \right). \quad (9)
$$

The combinations of parameters

$$
D_I = \frac{B_I}{2} - \mu_I \quad (10)
$$

and

$$
D_R = \frac{\rho B_R}{2} - \mu_R, \quad (11)
$$

entering respectively as input and output in DRS, are directly related with data, and are crucial for the determination of ρ, μ_R, B_R.

It must be noted that the usual direct evaluation of the exponential behavior in $d\sigma(t)/dt = (d\sigma(t)/dt)(t = 0) \times \exp(Bt)$ using a straight line for the measurements, actually informs the combined average

$$
B = 2\frac{D_I + \rho D_R}{1 + \rho^2} = \frac{(B_I - 2\mu_I) + \rho(\rho B_R - 2\mu_R)}{1 + \rho^2}. \quad (12)
$$

In a complete analysis of data all quantities in this expression, and not only the average slope B in $d\sigma/dt$, must be determined.

The forms written above for $T_I(t)$ and $T_R(t)$ are representations valid for small $|t|$, of amplitudes for the full t range, studied in several models [3,7] at ISR/CERN and higher energies that stress the peculiar properties of the real part of the elastic amplitude with common features of strong slope B_R and a zero for small $|t|$. In the low energy region here studied, there are not sufficient data for large $|t|$, and the analysis is restricted to the forward forms of Eqs. (3) and (4), showing that all quantities (for pp and $p\bar{p}$) in these expressions are necessary and sufficient for the description of data obeying constraints from DRA and DRS.

At very low energies, namely below $p_{\text{LAB}} = 4$ GeV, the description of elastic processes is influenced by details of

quark-quark and quark-antiquark interactions, with account for specific intermediate states, as for example in a framework of partial waves [17]. The measurement of polarized amplitudes [18], not considered here, depend on the precise values of nonpolarized quantities, as we obtain in the present work. In the energy range of our study, gluonic interactions are present, with global dynamics that is describable by simple analytical forms in the variables s, t.

With total cross sections, imaginary slopes and the linear terms μ_I written as analytical forms with powers and logarithms in the energy, both DRA and DRS require evaluation of principal value (PV) integrals with the generic structure

$$I(n, \lambda, x) = \mathbf{P} \int_1^{+\infty} \frac{x'^\lambda \log^n(x')}{x'^2 - x^2} dx'. \quad (13)$$

In recent studies, we have obtained the analytic exact solution for these integrals in terms of the Lerch's transcendents [14], and these solutions are applied in the present work, with demonstration that they are of fundamental importance, particularly in the low energy range.

The mathematical formalism of our work is presented in Sec. II and the energy dependent inputs of the imaginary parts are written, with forms that are shown to be valid up to LHC energies and also predict correctly the integrated elastic cross sections.

In Appendix A we calculate the phase of the nuclear-Coulomb interference for real amplitude of the form of Eq. (3).

In Appendix B we present in explicit form the calculation of dispersion relations for the amplitudes (DRA) and for their derivatives (DRS) with the exact solutions in terms of Lerch's transcendents.

In Appendix C we present alternative equivalent formalism for the total cross section in the language of Pomeron and Reggeon trajectories.

With established energy dependent inputs $\sigma(pp, p\bar{p})$, $B_I(pp, p\bar{p})$, $\mu_I(pp, p\bar{p})$ we give in Sec. III a precise description of the forward range of elastic pp and $p\bar{p}$ scattering, with the essential identification and separation of the real and imaginary amplitudes, with coherence and regularity in the energy dependence of all quantities.

In Sec. IV we present conclusions and summarize achievements of our effort.

II. FORMALISM AND INPUTS FOR DISPERSION RELATIONS

A. Inputs for imaginary part of elastic amplitude

In this section we introduce the forms of the imaginary part of the elastic amplitudes, and explain the determination of their parameters. We stress that we only use qualified data on $d\sigma/dt$ that may be considered as able to allow

reliable analysis in terms of amplitudes written in the analytical forms of Eqs. (3) and (4). The method of construction of our proposal is interactive, with inputs and outputs nourishing each other. In a first free analysis, we obtain values of parameters for σ, B_I and μ_I, while the quantities of the real part are left free. The extracted values are put in regular behavior with the energy, leading to analytical forms with terms of powers and logarithms as described below. Adopting these representations for the imaginary amplitude, we use exact forms of dispersion relations for amplitudes (DRA) and for slopes (DRS) to obtain the quantities of the real part, and then we review the imaginary amplitude.

In the reported experiments at low energies the momentum in the lab system p_{LAB} is more often used, while at high energies the use of the center of mass energy $\sqrt{s}$ is more common. For pp and $p\bar{p}$ scattering the connection with the lab energy

$$E = \sqrt{p_{LAB}^2 + m^2} \quad (14)$$

is

$$s = 2mE + 2m^2, \quad (15)$$

where m is the $p/\bar{p}$ mass. To work with the dispersion relations, the most useful quantity is the dimensionless ratio

$$x = E/m \quad (16)$$

and then

$$\frac{s}{2m^2} = x + 1. \quad (17)$$

Approximate relations that are often used at high energies are obviously $s \approx 2mE$, $x \approx s/2m^2$, $x \approx p_{LAB}/m$.

The usual parametrizations [13] for the total cross sections of the pp and $p\bar{p}$ interactions have the forms

$$\sigma^\mp(s) = P + H \log^2\left(\frac{s}{s_0}\right) + R_1\left(\frac{s}{s_0}\right)^{-\eta_1} \pm R_2\left(\frac{s}{s_0}\right)^{-\eta_2}, \quad (18)$$

with parameters P, H, R_1, R_2 constants given in millibarns, s_0 in GeV^2, while η_1, η_2 are dimensionless. The upper and lower indices $-,+$ refer to pp and $p\bar{p}$ scattering respectively. The representation is considered to be adequate for all energies $s \geq s_0$ and is based on a large number of values of $\sigma(pp, p\bar{p})$ found in experimental papers. We have the radical claim that these values often are not of good precision, for several reasons, and in general because the optical theorem is not applied to well identified imaginary amplitudes.

This form of amplitude is based on the Pomeron/Reggeon dynamics assumed for the strong interactions

TABLE I.   Parameters of total cross section, slopes and linear terms of imaginary parts in Eqs. (19), (21), and (22).

$\sigma(x)$					
P(mb)	H(mb)	R_1(mb)	R_2(mb)	η_1	η_2
34.37 ± 0.13	0.272 ± 0.00	12.74 ± 0.09	8.143 ± 0.180	0.4288 ± 0.0100	0.6144 ± 0.0090
$B_I(x)$					
b_0(GeV^{-2})	b_1(GeV^{-2})	b_2(GeV^{-2})	b_3(GeV^{-2})	b_4(GeV^{-2})	η_3	η_4
13.79 ± 0.12	-0.625 ± 0.070	0.04255 ± 0.01000	-6.937 ± 0.120	11.95 ± 0.21	0.5154 ± 0.0060	0.772 ± 0.006
$\mu_I(x)$					
μ_0(GeV^{-2})	μ_1(GeV^{-2})	$\cdots$	$\cdots$	$\cdots$	$\cdots$	$\cdots$
0.3724 ± 0.0096	-0.1441 ± 0.0021	$\cdots$	$\cdots$	$\cdots$	$\cdots$	$\cdots$

[2], and refers only to purely elastic processes. Contributions of diffractive nature, as first studied by Gribov and later formulated by Good and Walker [19], are not included in this framework. Single diffractive, double diffractive and truly inelastic processes have not been measured in the energy range of our study, while theoretical [8] work based on the gluonic dynamics of QCD and measurements start at energies of the ISR/CERN and Fermilab experiments [4], namely $\sqrt{s} \gtrsim 30$ GeV. We show indeed that our treatment describes well the integrated elastic and total cross sections at these higher energies.

Dispersion relations are defined with respect to the lab system energy, and, for low energies, terms like $\log^2(E+m)$ and $(E+m)^{-\eta}$ appear preventing to obtain closed exact forms. We then obtain a representation for the total cross sections in terms of dimensionless variables $x = E/m$, $x_0 = E_0/m$, with $x > 1$, writing

$$\sigma^\mp(x) = P + H \log^2\left(\frac{x}{x_0}\right) + R_1\left(\frac{x}{x_0}\right)^{-\eta_1} \pm R_2\left(\frac{x}{x_0}\right)^{-\eta_2},$$
(19)

and analyze all $d\sigma/dt$ data for $\mathrm{p_{LAB}}$ from 4 to 500 GeV/c using the assumed structures of the amplitudes in Eqs. (3) and (4).

We keep the value $s_0 = 16$ GeV^2 suggested [13] for Eq. (18), now appearing as

$$x_0 = s_0/(2m^2) = 9.0741,$$
(20)

where $m = 0.93827$ GeV. With this choice, the parameters P, H, R_1, R_2 remain the same and numerical values are the same, given in Table I. With

$$(\hbar c)^2 = 0.38938 \ \mathrm{GeV^2 \ mb}$$

we also need

$$(\hbar c)^2 \frac{1}{m^2} = 0.4423 \ \mathrm{mb}.$$

In Fig. 1 we show the comparison between Eqs. (18) and (19) for $p\bar{p}$ written with the same parameters. The

difference between the curves represents the deviation of Eq. (17) to the approximated form $x \approx s/2m^2$.

For use as inputs in dispersion relations DRS we write the slopes $B_I^{pp}(x)$ and $B_I^{p\bar{p}}(x)$ in terms of the x variable as

$$B_I^\mp(x) = b_0 + b_1 \log x + b_2 \log^2 x + b_3 x^{-\eta_3} \pm b_4 x^{-\eta_4},$$
(21)

again with symmetry in the coefficients for $p\bar{p}$ and pp. As in Eqs. (18) and (19), for $s/2m^2 \gg 1$ the slopes B_I of Eq. (21) can be written with similar analytical forms in the variable s.

In Eq. (4) we have in addition to the slope of the imaginary part, B_I, a term μ_I which is linear on t dependence. The inputs $\mu_I(x)$ for both pp and $p\bar{p}$ are determined by a controlled analysis. The result is that the difference between the values of $\mu_I(x)$ for pp and $p\bar{p}$ is not important, and we assume for both the form

$$\mu_I^\mp(x) = \mu_0 + \mu_1 \log x.$$
(22)

The numerical values of the input parameters are given in Table I and in Fig. 2 we show the quantities $\sigma(x)$, $B_I(x)$ and
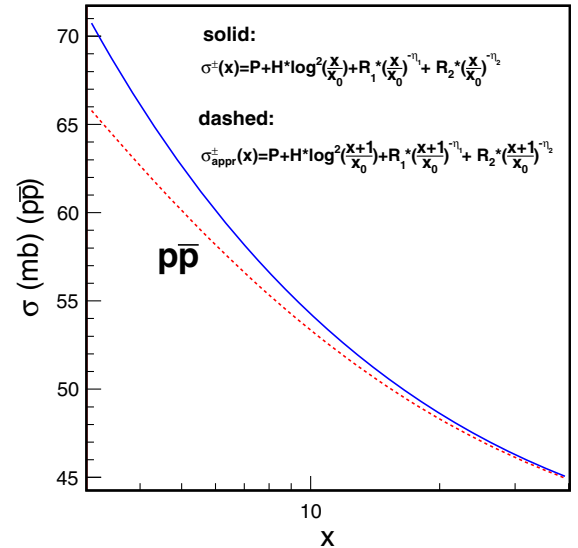

FIG. 1.   Comparison between calculations of $p\bar{p}$ cross sections with Eqs. (18) and (19) using the same parameter values, showing the deviation for low energies due to kinematics.
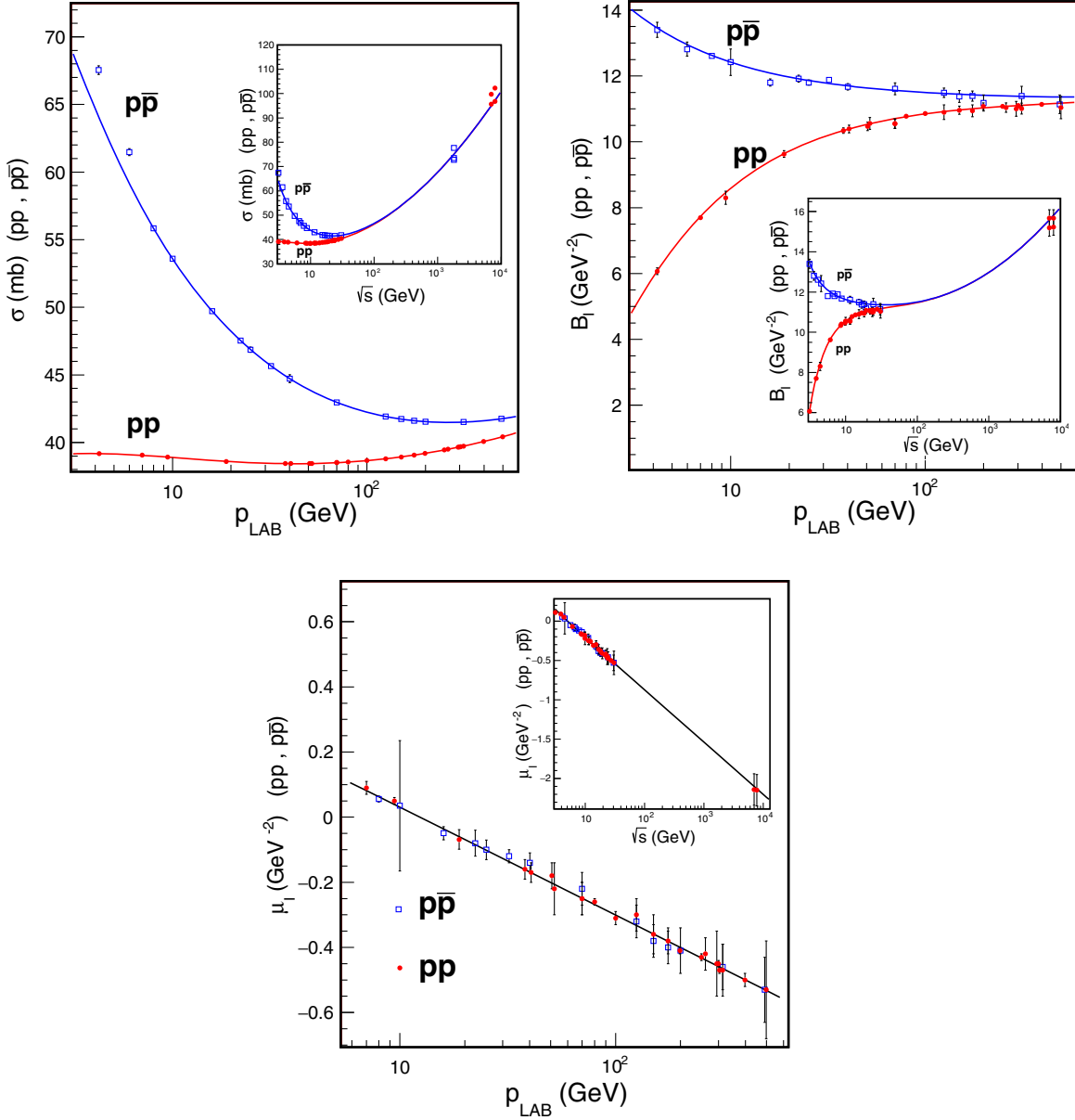
FIG. 2.   Input forms for σ, B_I and μ_I of Eqs. (19), (21), and (22), together with values obtained in the study of the data in Sec. III. The connections of the analytical forms with our previously published calculations [7] for very high energies (1.8 TeV and LHC) are shown in the insets in terms of $\sqrt{s}$.

$\mu_I(x)$ of Eqs. (19), (21), and (22) with the points obtained in the examination of the data described in Sec. III. In the inset plots with the variable $\sqrt{s}$ we show that the extrapolations up to LHC energies (7 and 8 TeV) are compatible with the predicted results [7,10].

The integrated elastic cross section of the imaginary part is given by

$$\frac{\sigma_I^{\text{el}}}{\sigma}(x) = \frac{1}{\sigma}\int_0^{-\infty}\frac{d\sigma_I}{dt}$$
$$= \frac{1}{16\pi(\hbar c)^2}\frac{\sigma}{B_I}\left[\left(1+\frac{\mu_I}{B_I}\right)^2 + \frac{\mu_I^2}{B_I^2}\right]. \quad (23)$$

Plots of $\sigma_I^{\text{elastic}}$ and the ratio with σ as a function of the energy are given in Fig. 3. We recall that this expression gives the ratio of the purely elastic processes. The remaining part of the ratio $1 - \sigma_I^{\text{el}}/\sigma$ gives diffractive plus inelastic processes. We also mark in the figure the experimental values of σ^{elastic} in the ISR range ($\sqrt{s} \approx 30$ to 60 GeV) [4] and our published calculations for 1.8 GeV and LHC energies [7].

The dimensionless Fourier transforms of the amplitude $T(s,t)$ in Eqs. (3) and (4). with respect to the momentum transfer

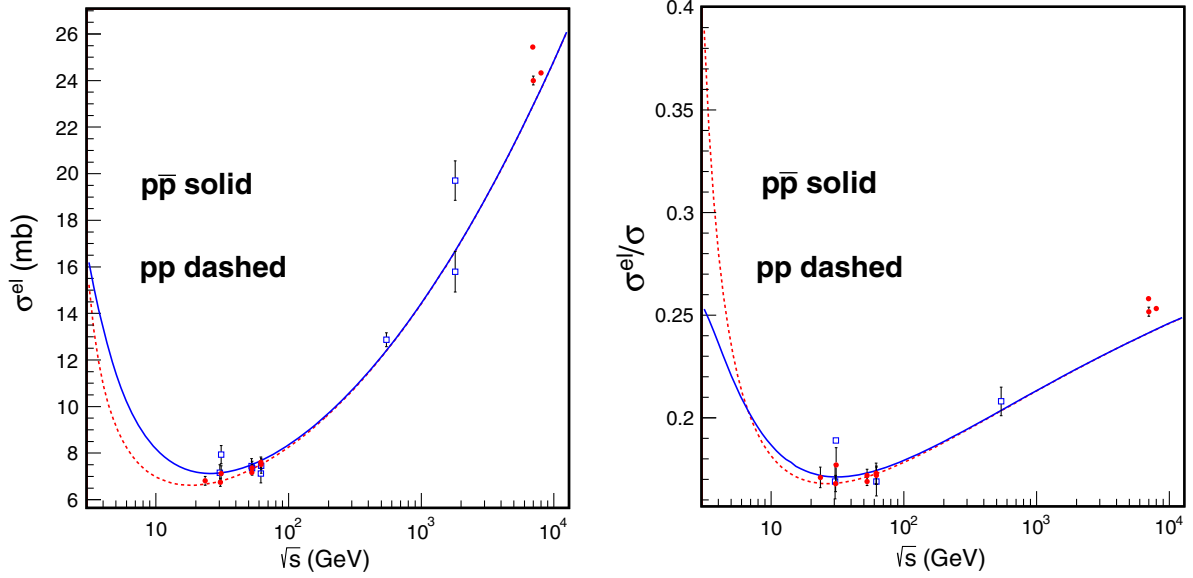$$\tilde{T}(b;s) = \tilde{T}_R + i\tilde{T}_I \quad (24)$$

FIG. 3.   (a) Integrated elastic cross section due to the imaginary part of the amplitude. Recall that the difference $\sigma - \sigma_I^{\text{elastic}}$ accounts for diffractive plus inelastic processes. The large difference indicates that diffractive processes are highly dominant at low energies. Experimental points [4] from ISR/CERN, Fermilab (1.8 TeV) and LHC (7 and 8 TeV) [5] are marked. (b) The same plot, for the ratio $\sigma_I^{\text{elastic}}/\sigma$. The agreement of the lines with the data points shown that our amplitudes are realistic.

are given by

$$\tilde{T}_R(b;s) = \frac{\sigma}{2\pi B_R}\left\{\rho + \frac{\mu_R}{B_R}\left(2 - \frac{b^2}{B_R}\right)\right\}e^{-b^2/2B_R} \quad (25)$$

and

$$\tilde{T}_I(b;s) = \frac{\sigma}{2\pi B_I}\left\{1 + \frac{\mu_I}{B_I}\left(2 - \frac{b^2}{B_I}\right)\right\}e^{-b^2/2B_I}. \quad (26)$$

The profile corresponding to the imaginary forward amplitude is dominant over the real part for low b values. However from $b \geq 14$ GeV ($\simeq 2.8$ fm) the real part can be dominant and this effect is more pronounced due to the presence of the μ_R parameter in Eq. (25).

In Appendix C alternative forms are written for the total cross section, $\sigma(x)$ or $\sigma(s)$, in terms of power instead of logarithm as in Donnachie-Landshoff formalism, with all accuracy.

B. Dispersion relations for amplitudes and slopes

The well known dispersion relations for pp and $p\bar{p}$ elastic scattering are written in terms of even and odd dimensionless amplitudes,

$$\text{Re}F_+(E,t) = K + \frac{2E^2}{\pi}\mathbf{P}\int_m^{+\infty}dE'\,\frac{\text{Im}F_+(E',t)}{E'(E'^2 - E^2)}, \quad (27)$$

$$\text{Re}F_-(E,t) = \frac{2E}{\pi}\mathbf{P}\int_m^{+\infty}dE'\,\frac{\text{Im}F_-(E',t)}{(E'^2 - E^2)}. \quad (28)$$

With $x = E/m$, the even and odd combinations of amplitudes are related to the pp and $p\bar{p}$ systems through

$$F_{pp}(x,t) = F_+(x,t) - F_-(x,t),$$
$$F_{p\bar{p}}(x,t) = F_+(x,t) + F_-(x,t). \quad (29)$$

The optical theorem informs the normalization of the amplitudes by

$$\sigma_{pp}(x) = \frac{\text{Im}F_{pp}(x,t=0)}{2m^2x} \quad (30)$$

and similarly for $p\bar{p}$.

With the exponential and linear factors in the imaginary parts, we write the inputs

$$\frac{\text{Im}F_{pp}(x,t)}{2m^2x} = \sigma_{pp}[1 - \mu_I^{pp}]\exp\left(B_I^{pp}t/2\right), \quad (31)$$

$$\frac{\text{Im}F_{p\bar{p}}(x,t)}{2m^2x} = \sigma_{p\bar{p}}[1 - \mu_I^{p\bar{p}}]\exp\left(B_I^{p\bar{p}}t/2\right), \quad (32)$$

with functions $\sigma(x)$, $B_I(x)$ and $\mu_I(x)$ for pp and $p\bar{p}$ given in Eqs. (19), (21), and (22).

As explained in Sec. I, the real parts are written with exponential and linear factors

$$\frac{\text{Re}F_{pp}(x,t)}{2m^2x} = \sigma_{pp}(x)[\rho_{pp}(x) - \mu_R^{pp}(x)t]\exp[B_R^{pp}(x)t/2]$$
$$(33)$$

and similarly for $p\bar{p}$.

The ρ parameters are then obtained from

$$\frac{1}{2m^2x}\text{Re}F_+(x,0) = \frac{1}{2}[(\sigma\rho)(p\bar{p}) + (\sigma\rho)(pp)] \quad (34)$$

and

$$\frac{1}{2m^2x}\text{Re}F_-(x,0) = \frac{1}{2}[(\sigma\rho)(p\bar{p}) - (\sigma\rho)(pp)], \quad (35)$$

with the lhs given by dispersion relations (27) and (28).

Thus the ρ parameter of the real part is defined by

$$\sigma_{pp}(x)\rho_{pp}(x) = \frac{\text{Re}F_{pp}(x,t=0)}{2m^2x}, \quad (36)$$

and similarly for $p\bar{p}$.

The derivatives of the real amplitude at $|t| = 0$ are written

$$\frac{\partial \text{Re}F_{pp}(x,t)}{\partial t}\bigg|_{t=0} = 2m^2x\sigma_{pp}(x)\left[\frac{\rho_{pp}B_R^{pp}}{2} - \mu_R^{pp}\right](x), \quad (37)$$

and similarly for $p\bar{p}$. These quantities are determined by DRS, which give the even and odd combinations

$$\frac{1}{2m^2x}\frac{\partial \text{Re}F_+(x,t)}{\partial t}\bigg|_{t=0} = \frac{1}{2}[\sigma_{p\bar{p}}D_R^{p\bar{p}} + \sigma_{pp}D_R^{pp}] \quad (38)$$

and

$$\frac{1}{2m^2x}\frac{\partial \text{Re}F_-(x,t)}{\partial t}\bigg|_{t=0} = \frac{1}{2}[\sigma_{p\bar{p}}D_R^{p\bar{p}} - \sigma_{pp}D_R^{pp}]. \quad (39)$$

The quantities $D_R^{p\bar{p}}$ and D_R^{pp} are combinations of amplitude parameters as in Eq. (11).

Substituting these expressions into Eqs. (27) and (28), written in terms of the dimensionless variable x, we obtain

$$\text{Re}F_+(x,t) = K + \frac{2m^2x^2}{\pi}\mathbf{P}\int_1^{+\infty}\frac{1}{x'^2 - x^2}$$
$$\times [\sigma_{p\bar{p}}(x')(1 - \mu_I^{p\bar{p}}(x'))\exp[B_I^{p\bar{p}}(x')t/2]$$
$$+ \sigma_{pp}(x')(1 - \mu_I^{pp}(x'))\exp[B_I^{pp}(x')t/2]]dx' \quad (40)$$

and

$$\text{Re}F_-(x,t) = \frac{2m^2x}{\pi}\mathbf{P}\int_1^{+\infty}\frac{x'}{x'^2 - x^2}[\sigma_{p\bar{p}}(x')(1 - \mu_I^{p\bar{p}}(x'))$$
$$\times \exp[B_I^{p\bar{p}}(x')t/2] - \sigma_{pp}(x')(1 - \mu_I^{pp}(x'))$$
$$\times \exp[B_I^{pp}(x')t/2]]dx'. \quad (41)$$

Taking $t = 0$ we obtain the dispersion relations for the amplitudes (DRA)

$$\text{Re}F_+(x,t=0) = 2m^2x[\sigma_{p\bar{p}}\rho_{p\bar{p}} + \sigma_{pp}\rho_{pp}](x)$$
$$= K + \frac{2m^2x^2}{\pi}\mathbf{P}\int_1^{+\infty}\frac{1}{x'^2 - x^2}$$
$$\times [\sigma_{p\bar{p}} + \sigma_{pp}](x')dx' \quad (42)$$

and

$$\text{Re}F_-(x,t=0) = 2m^2x[\sigma_{p\bar{p}}\rho_{p\bar{p}} - \sigma_{pp}\rho_{pp}](x)$$
$$= \frac{2m^2x}{\pi}\mathbf{P}\int_1^{+\infty}\frac{x'}{x'^2 - x^2}[\sigma_{p\bar{p}} - \sigma_{pp}](x')dx'. \quad (43)$$

The expressions in terms of PV integrals are given in Appendix B.

To obtain DRS, we take derivatives of Eqs. (40) and (41) with respect to t, writing

$$\frac{\partial \text{Re}F_+(x,t)}{\partial t} = \frac{m^2x^2}{\pi}\mathbf{P}\int_1^{+\infty}\frac{1}{x'^2 - x^2}$$
$$\times [\sigma_{p\bar{p}}(x')[B_I^{p\bar{p}} - 2\mu_I^{p\bar{p}}](x')\exp[B_I^{p\bar{p}}(x')t/2]$$
$$+ \sigma_{pp}(x')[B_I^{pp}(x') - 2\mu_I^{pp}(x')]$$
$$\times \exp[B_I^{pp}(x')t/2]]dx', \quad (44)$$

$$\frac{\partial \text{Re}F_-(x,t)}{\partial t} = \frac{m^2x}{\pi}\mathbf{P}\int_1^{+\infty}\frac{x'}{x'^2 - x^2}$$
$$\times [\sigma_{p\bar{p}}(x')[B_I^{p\bar{p}} - 2\mu_I^{p\bar{p}}](x')\exp[B_I^{p\bar{p}}(x')t/2]$$
$$- \sigma_{pp}(x')[B_I^{pp}(x') - 2\mu_I^{pp}(x')]$$
$$\times \exp[B_I^{pp}(x')t/2]]dx'. \quad (45)$$

With $t = 0$, these equations become the dispersion relations for slopes (DRS) that we may write

$$4[\sigma_{p\bar{p}}D_R^{p\bar{p}} + \sigma_{pp}D_R^{pp}](x)$$
$$= \frac{x}{\pi}\mathbf{P}\int_1^{+\infty}\frac{2}{x'^2 - x^2}[\sigma_{p\bar{p}}D_I^{p\bar{p}} + \sigma_{pp}D_I^{pp}(x')](x')dx', \quad (46)$$

$$4[\sigma_{p\bar{p}}D_R^{p\bar{p}} - \sigma_{pp}D_R^{pp}](x)$$
$$= \frac{1}{\pi}\mathbf{P}\int_1^{+\infty}\frac{2x'}{x'^2 - x^2}[\sigma_{p\bar{p}}D_I^{p\bar{p}} - \sigma_{pp}D_I^{pp}](x')dx', \quad (47)$$

where we have introduced the parametrization of the real amplitudes.

TABLE II.   Values of parameters of μ_R for pp and $p\bar{p}$ in Eqs. (50) and (51), obtained for $K = -310$. The corresponding lines are shown in Fig. 5. The central values of c_0 and c_2 are shown with high precision to put coincident the zeros of ρ and $D_R/2 + \mu_R$ for the choice $K = -310$.

pp			
$c_0 (\text{GeV}^{-2})$	ν_1	$c_1 (\text{GeV}^{-2})$	$c_2 (\text{GeV}^{-2})$
1.897 ± 0.160	0.450 ± 0.032	-17.87 ± 0.92	-0.142 ± 0.001
$p\bar{p}$			
$c_3 (\text{GeV}^{-2})$	ν_4	$c_4 (\text{GeV}^{-2})$	$c_5 (\text{GeV}^{-2})$
0.653 ± 0.121	0.385 ± 0.101	-4.71 ± 0.74	-0.075 ± 0.001

In Eqs. (47) and (48) the terms D_I^{pp} and $D_I^{p\bar{p}}$ given by Eq. (10) keep analytical form similar to that of $B_I(x)$ given by Eq. (21), since the parametrization of μ_I is linear in $\log(x)$. The presence of the quantity $\mu_I(x)$ as an input in dispersion relations for slopes does not change the algebra of Eqs. (B10) and (B11) (which were first written [14] assuming $\mu_I = 0$) and the contribution of μ_I can be given by the change of the parameters

$$b_0 \rightarrow b_0' = b_0 - 2\mu_0,$$
$$b_1 \rightarrow b_1' = b_1 - 2\mu_1. \tag{48}$$

Introducing analytical expressions for the terms in the imaginary parts, we fall in principal value integrations of the form (B1) that we can solve exactly [14]. The input forms in Eqs. (19), (21) and (22) taken into the expressions from DRA and DRS, with numbers given in Sec. III lead to values for ρ and the coefficients of the derivatives of the real parts at the origin D_R for pp and $p\bar{p}$. In the low energy end, namely with p_{LAB} up to 30 GeV, it is essential to use the exact solutions for the PV integrals that appear in DRA and DRS in the calculations of ρ and D_R. Illustrating plots are given in Appendix B.

From comparison of the results with the ρ data, the value of the separation constant K that appears in the expressions of DRA is determined. We obtain the interval

$$K = \text{from} \,(-310)\, \text{to} \,(-287). \tag{49}$$

In the examples and plots of the present paper we use the value $K = -310$.

Given the $\sigma(x)$, $B_I(x)$ and μ_I inputs, the quantities ρ and D_R are determined by DRA and DRS. Since $D_R = \rho B_R/2 - \mu_R$ is a combination of μ_R and B_R, they must be determined by the data. We obtain that μ_R presents very regular energy dependence for both pp and $p\bar{p}$ systems. We introduce the forms

$$\mu_R(pp) = c_0 + c_1 x^{-\nu_1} + c_2 \log x \tag{50}$$

and

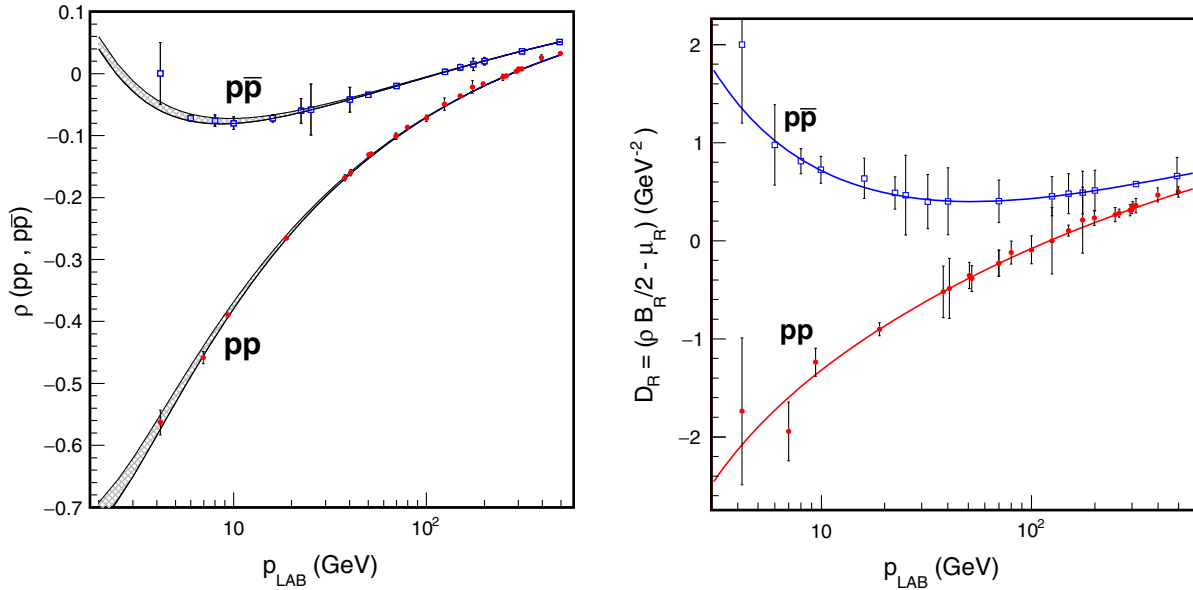$$\mu_R(p\bar{p}) = c_3 + c_4 x^{-\nu_4} + c_5 \log x. \tag{51}$$

FIG. 4.   (a) The lines give the predictions for the quantity ρ predicted by dispersion relations for the amplitudes DRA, showing the band with variation of K from -310 to -287. The marked points are obtained from the data. It is important to remark that the positions of the ρ zeros $|t|_0(pp) = 276.91$ GeV^2 and $|t|_0(p\bar{p}) = 116.93$ GeV^2 predicted by DRA are confirmed by the data. (b) The lines show the predictions from the dispersion relations for slopes DRS for the derivatives of the real amplitudes at the origin, which are represented by the combinations $D_R = \rho B_R/2 - \mu_R$ for pp and $p\bar{p}$. The marked points represent these combinations of parameters ρ, μ_R, B_R calculated with the values for the experimental data presented in Sec. III.
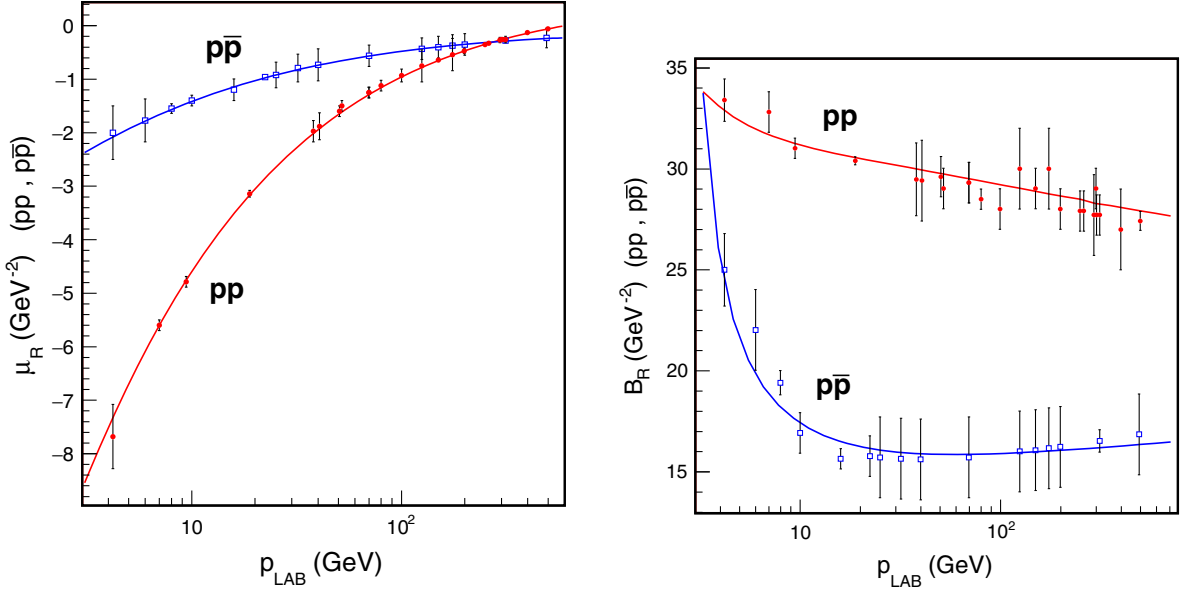
FIG. 5. (a) Representations of the values of the parameters μ_R^{pp} and $\mu_R^{p\bar{p}}$ through Eqs. (50) and (51) and the points obtained from the data. (b) Energy dependence of the slopes $B_R(pp)$ and $B_R(p\bar{p})$ of the real amplitudes. The lines are fully predicted by the dispersion relations for slopes DRS (that give $D_R = \rho B_R/2 - \mu_R$ for pp and $p\bar{p}$), dispersion relations for the amplitudes (that give ρ for pp and $p\bar{p}$) and by Eqs. (50) and (51) that give μ_R^{pp} and $\mu_R^{p\bar{p}}$.

Numerical values for the constants are given in Table II and plots are shown in Fig. 5.

C. Output quantities and plots

We must compare the results that are given in Sec. III with the predictions from dispersion relations for the quantities of the real part ρ, D_R and μ_R for the pp and $p\bar{p}$ systems. Figure 4 shows the energy dependence of the predictions from DRA and DRS for ρ and for the derivative coefficient $D_R = \rho B_R/2 - \mu_R$.

In Fig. 5(a) we show the energy dependence obtained for the parameter μ_R for pp $p\bar{p}$ and in Fig. 5(b) we form the quotient $B_R = 2(D_R + \mu_R)/\rho$ using as point values shown in the large table with fit results, and the lines are calculated with Eqs. (50) and (51) and the analytical results for ρ and D_R (pp and $p\bar{p}$) from DRA and DRS. Note that the points where ρ passes by zero must coincide with the zero of the sum $D_R + \mu_R$. This condition results naturally in our solution.

We thus have a closed coherent determination of all quantities describing forward scattering, with no free local parameter.

III. ANALYSIS OF DATA IN FORWARD DIRECTION

The data [20] presented in Tables III and IV cover $|t|$ ranges accessible for the analysis, which requires a regular set of points with $|t| \leq 0.5$ GeV^2. Ideally, it would be nice to have good quality data from the very low

$|t| \approx 0.001$ GeV^2 and going up to 0.1 GeV^2, but this is not always available in the low energy range.

The analysis covers all data of elastic pp and $p\bar{p}$ scattering in the energy range of $\sqrt{s}$ from 3 to 30 GeV. These data have been treated along the history with incomplete theoretical expressions for $d\sigma/dt$. In this energy range it is believed that the dynamics of forward scattering is mainly determined by gluonic interactions resulting in smooth energy dependence of all parameters. On the other hand, at very low energies below $p_{LAB} = 4$ GeV the direct quark-quark and quark-antiquark interactions may be more important. This seems to be particularly visible in the $p\bar{p}$ case.

Above $\sqrt{s} = 30$ GeV, ISR/CERN and Fermilab data, covering very wide t ranges, deserves to be studied with analytical forms including the whole t range. There are many models [3,7] for this purpose, and the forward scattering forms here studied are part of these full-$|t|$ descriptions.

An important feature of our analysis is the absorption of normalization errors that accompany the determinations of $d\sigma/dt$. Even when these normalization indeterminacies are small, their influence in the parameters is large. The experimental papers use criteria for normalization that we do not consider legal or correct, as ignoring existence of real part, ignoring realistic t dependences in the amplitudes, and comparison with other experiments. Some experiments report σ values using data that are not qualified for the analysis (as insufficient t range). These difficulties lead to fluctuations in values of parameters that do not represent physical effects and do not allow a regular global description.

TABLE III.　Values of the parameters for the amplitudes of pp elastic scattering.

p_{LAB} (GeV)	$\sqrt{s}$ (GeV)	N	$t_{min}-t_{max}$ (GeV^{-2})	f	σ (mb)	$B_I-2\mu_I$ (GeV^{-2})	ρ	B_R (GeV^{-2})	μ_R (GeV^{-2})	μ_I (GeV^{-2})	χ^2	Re [20]
4.2	3.14	39	0.001 06–0.189	1.0520	39.18 ± 0.16	5.85 ± 0.08	−0.564 ± 0.020	33 ± 1	−7.68 ± 0.69	0.11 ± 0.03	1.165	aq
7	3.88	59	0.001 41–0.31	1.0316	39.05 ± 0.08	7.52 ± 0.04	−0.460 ± 0.010	33 ± 1	−5.60 ± 0.10	0.09 ± 0.02	1.87	aq
9.43	4.42	34	0.000 79–0.01283	0.9966	38.92 ± 0.09	8.2 ± 0.2	−0.390 ± 0.002	31 ± 1	−4.8 ± 0.1	0.05 ± 0.01	1.042	h
18.9	6.11	67	0.0009–0.10883	0.9845	38.6 ± 0.04	9.76 ± 0.08	−0.266 ± 0.001	30 ± 1	−3.14 ± 0.06	−0.07 ± 0.03	1.227	h
38.01	8.55	65	0.000 86–0.113 18	0.9792	38.44 ± 0.02	10.37 ± 0.06	−0.160 ± 0.004	30 ± 2	−1.99 ± 0.25	−0.13 ± 0.03	1.282	h
40.62	8.83	65	0.000 88–0.113 79	0.9916	38.44 ± 0.04	10.73 ± 0.1	−0.161 ± 0.005	29 ± 2	−1.88 ± 0.25	−0.17 ± 0.03	1.55	h
42.5	9.03	19	0.001 93–0.039 82	1.0007	38.43 ± 0.25	10.90 ± 0.20	−0.160 ± 0.010	30 ± 1	−1.60 ± 0.30	−0.25 ± 0.30	0.762	j
50.62	9.84	66	0.000 96–0.115 08	0.9728	38.44 ± 0.05	10.83 ± 0.1	−0.132 ± 0.004	30 ± 1	−1.6 ± 0.1	−0.18 ± 0.04	1.651	h
52	9.97	72	0.000 63–0.0306	0.9800	38.45 ± 0.06	11 ± 0.08	−0.130 ± 0.004	29 ± 1	−1.5 ± 0.1	−0.22 ± 0.08	1.297	i
52.2	9.99	18	0.001 87–0.050 41	0.9903	38.45 ± 0.20	11.30 ± 0.30	−0.132 ± 0.020	29 ± 2	−1.50 ± 0.10	−0.22 ± 0.20	1.729	j
69.84	11.53	73	0.001 11–0.108 17	1.0094	38.51 ± 0.06	11.05 ± 0.1	−0.101 ± 0.005	29 ± 1	−1.25 ± 0.1	−0.25 ± 0.05	1.238	h
70	11.54	124	0.001 85–0.083 52	1.0038	38.51 ± 0.07	11.05 ± 0.1	−0.101 ± 0.005	29 ± 1	−1.25 ± 0.1	−0.25 ± 0.05	0.888	n
80	12.32	58	0.000 66–0.029 28	0.9953	38.55 ± 0.06	11.3 ± 0.04	−0.087 ± 0.004	29 ± 1	−1.12 ± 0.1	−0.26 ± 0.01	0.960	i
100	13.76	140	0.001 70–0.151 13	1.0053	38.66 ± 0.06	11.48 ± 0.03	−0.073 ± 0.005	28 ± 1	−0.93 ± 0.12	−0.31 ± 0.02	1.054	n
100	13.76	73	0.0022–0.0388	1.0045	38.66 ± 0.07	11.48 ± 0.03	−0.073 ± 0.005	28 ± 1	−0.93 ± 0.12	−0.31 ± 0.02	1.252	r
125	15.37	92	0.001 64–0.098 28	1.0158	38.8 ± 0.05	11.5 ± 0.2	−0.05 ± 0.01	30 ± 2	−0.75 ± 0.3	−0.3 ± 0.05	0.845	n
150	16.83	92	0.001 64–0.098 28	0.9943	38.93 ± 0.06	11.68 ± 0.02	−0.037 ± 0.003	29 ± 1	−0.64 ± 0.03	−0.36 ± 0.06	1.198	n
150	16.83	68	0.0022–0.0392	0.9920	38.93 ± 0.06	11.68 ± 0.02	−0.037 ± 0.003	29 ± 1	−0.64 ± 0.03	−0.36 ± 0.06	1.192	r
175	18.17	55	0.001 81–0.097 66	1.0103	39.07 ± 0.07	11.7 ± 0.16	−0.022 ± 0.01	30 ± 2	−0.54 ± 0.3	−0.38 ± 0.04	1.152	n
199	19.37	69	0.000 66–0.0315	0.988	39.2 ± 0.06	11.9 ± 0.1	−0.017 ± 0.004	28 ± 1	−0.47 ± 0.05	−0.41 ± 0.01	1.143	i
250	21.7	64	0.0022–0.039	0.9880	39.45 ± 0.06	11.94 ± 0.01	−0.006 ± 0.005	28 ± 1	−0.35 ± 0.02	−0.43 ± 0.01	0.712	r
261	22.17	63	0.0005–0.029 78	0.994	39.5 ± 0.06	11.88 ± 0.1	−0.0034 ± 0.002	28 ± 1	−0.33 ± 0.03	−0.42 ± 0.05	1.291	i
294.4	23.54	31	0.000 37–0.0102	1.0118	39.65 ± 0.08	11.9 ± 0.1	0.003 ± 0.002	28 ± 2	−0.27 ± 0.05	−0.45 ± 0.1	0.608	k
300	23.76	60	0.0022–0.0388	0.9941	39.67 ± 0.08	12 ± 0.03	0.004 ± 0.002	29 ± 1	−0.26 ± 0.03	−0.45 ± 0.01	1.078	r
303.1	23.88	66	0.000 66–0.0316	0.9823	39.69 ± 0.06	12.03 ± 0.03	0.007 ± 0.003	28 ± 1	−0.26 ± 0.01	−0.47 ± 0.01	1.295	i
313.7	24.3	31	0.001 08–0.013 13	1.0054	39.73 ± 0.05	11.95 ± 0.05	0.007 ± 0.003	28 ± 1	−0.26 ± 0.06	−0.47 ± 0.08	0.763	l
398	27.36	60	0.000 47–0.025 79	0.979	40.07 ± 0.07	12.14 ± 0.01	0.025 ± 0.005	27 ± 2	−0.13 ± 0.01	−0.50 ± 0.02	1.272	i
499.1	30.63	32	0.0005–0.0176	1.0080	40.43 ± 0.05	12.1 ± 0.15	0.032 ± 0.003	27 ± 2	−0.06 ± 0.01	−0.53 ± 0.15	0.776	k

After a smooth description has been achieved and parameters P, H, R_1, R_2, η_1, η_2 of Eq. (19) are determined, the values of σ are imposed at each energy. Thus we introduce a constant normalization factor f for each data set, chosen so that the total cross section σ equals the value determined given by Eq. (19). We thus write

$$\frac{d\sigma}{dt} = f \times \frac{d\sigma}{dt}\Big|_{\text{data}}. \qquad (52)$$

TABLE IV.　Values of the parameters for the amplitudes of $p\bar{p}$ elastic scattering.

p_{LAB} (GeV)	$\sqrt{s}$ (GeV)	N	$t_{min}-t_{max}$ (GeV^{-2})	f	σ (mb)	$B_I-2\mu_I$ (GeV^{-2})	ρ	B_R (GeV^{-2})	μ_R (GeV^{-2})	μ_I (GeV^{-2})	χ^2	Re [20]
4.2	3.14	48	0.001 06–0.54	1	67.45 ± 0.32	13.4 ± 0.11	0 ± 0.05	25 ± 2	−2 ± 0.5	0 ± 0.1	1.33	aq
6	3.63	83	0.001 41–0.42	1	61.44 ± 0.26	12.8 ± 0.08	−0.072 ± 0.005	22 ± 2	−1.77 ± 0.4	0 ± 0.1	1.331	ab
8	4.11	83	0.001 81–0.33	1.021	55.84 ± 0.05	12.5 ± 0.02	−0.076 ± 0.009	19 ± 1	−1.55 ± 0.09	0.056 ± 0.009	1.567	ac
10	4.54	55	0.001 81–0.355	1	53.6 ± 0.1	12.35 ± 0.05	−0.08 ± 0.01	17 ± 1	−1.4 ± 0.1	0.035 ± 0.2	1.106	ad
16	5.64	25	0.085–0.540	1.1084	49.71 ± 0.18	11.90 ± 0.10	−0.072 ± 0.006	16 ± 1	−1.2 ± 0.2	−0.05 ± 0.02	2.84	c
22.4	6.62	32	0.055–0.43	1.0242	47.53 ± 0.12	12.08 ± 0.07	−0.060 ± 0.020	16 ± 1	−0.96 ± 0.04	−0.08 ± 0.04	0.771	g
25.2	7.01	33	0.075–0.580	1.0914	46.87 ± 0.20	12.00 ± 0.05	−0.058 ± 0.041	16 ± 2	−0.92 ± 0.24	−0.10 ± 0.03	1.562	e
32.1	7.88	39	0.055–0.47	1.0950	45.66 ± 0.17	12.00 ± 0.05	−0.050 ± 0.010	16 ± 2	−0.80 ± 0.26	−0.14 ± 0.02	3.285	s
40.1	8.78	30	0.075–0.520	1.1306	44.72 ± 0.30	11.90 ± 0.08	−0.042 ± 0.020	16 ± 2	−0.73 ± 0.3	−0.14 ± 0.03	2.362	e
50	9.78	11	0.0375–0.400	1.0136	43.93 ± 0.20	11.58 ± 0.08	−0.036 ± 0.020	13 ± 1.5	−0.66 ± 0.10	−0.18 ± 0.02	2.114	f
70	11.54	125	0.001 85–0.084 68	1.0076	42.97 ± 0.11	12.05 ± 0.15	−0.02 ± 0.02	16 ± 2	−0.56 ± 0.2	−0.22 ± 0.05	1.279	n
70	11.54	125	0.0375–0.500	1.0076	42.97 ± 0.11	12.05 ± 0.15	−0.02 ± 0.02	16 ± 2	−0.56 ± 0.2	−0.22 ± 0.05	1.279	f
125	15.37	140	0.001 64–0.209 31	1.0101	41.92 ± 0.08	12.13 ± 0.1	0.003 ± 0.001	16 ± 2	−0.43 ± 0.2	−0.32 ± 0.05	1.206	n
150	16.83	140	0.001 64–0.209 31	0.996	41.73 ± 0.11	12.14 ± 0.15	0.01 ± 0.005	16 ± 2	−0.4 ± 0.2	−0.38 ± 0.05	1.205	n
175	18.17	86	0.001 81–0.097 66	1.0019	41.61 ± 0.14	12.19 ± 0.12	0.015 ± 0.01	16 ± 2	−0.37 ± 0.2	−0.4 ± 0.05	1.051	n
175	18.17	86	0.0375–0.600	1.0019	41.61 ± 0.14	12.19 ± 0.12	0.015 ± 0.01	16 ± 2	−0.37 ± 0.2	−0.4 ± 0.05	1.051	f
200	19.42	86	0.001 81–0.536 56	1.0125	41.54 ± 0.09	12 ± 0.2	0.02 ± 0.006	16 ± 2	−0.35 ± 0.2	−0.41 ± 0.07	1.359	n
313.7	24.3	32	0.001 08–0.013 76	0.9911	41.51 ± 0.04	12.31 ± 0.26	0.036 ± 0.002	17 ± 1	−0.28 ± 0.01	−0.46 ± 0.07	0.51	l
491.5	30.4	29	0.000 67–0.015 61	0.9859	41.76 ± 0.15	12.2 ± 0.2	0.051 ± 0.003	17 ± 2	−0.23 ± 0.18	−0.53 ± 0.1	1.525	k

The value of f for the data set of each experiment is given in Tables III and IV. Thus the central values of σ are assumed and f is determined. The error bars in σ and other quantities represent sensitivities of the fit to each parameter individually, without freedom for correlations.

The resulting suggested parameter values from our analysis are collected in Tables III and IV. The input energies for the data are written primarily in terms of p_{LAB}, as has been more usual in the presentation of data in this range, but the table also includes $\sqrt{s}$ values. In some cases, mainly at very low energies, where data are not rich, we combine information from different experiments of same or nearby energies, in the same numerical treatment and in plots. We observe good matching of data sets.

We show examples of the treatment of the $d\sigma/dt$ data in many plots. More detailed information is given in the figure captions. The log $|t|$ horizontal scale helps to expand and exhibit the small $|t|$ behavior, and it is remarkable that often the descriptions work very well up to $|t| = 0.2$, beyond the strictly forward range that determines parameters. We interpret that this is so thanks to appropriate form assumed for the amplitudes, and to the control established by DRA and DRS.

Ranges where ρ passes by zero are particularly delicate. The experiments at $\sqrt{s} = 23.542$ and 23.882 GeV ($p_{LAB} = 294.4$ and 303.1 GeV) give an example in which there is discrepancy in literature for the ρ sign. Our treatment solves the discrepancy, namely we show that ρ passes by zero in this region, and this is valid for both experiments. Parameters are in Table III.

For $p\bar{p}$ in the range of our analysis ρ is always small and the data are poor. We are then strongly dependent on the predictions from DRA and DRS.

We inspect and analyze the data using a CERN MINUIT program for the determination of χ^2, nominally with six parameters. We use the form for the total pp and $p\bar{p}$ cross sections in Eq. (19), and iteratively with observations of the behavior of B_I and μ_I, and use of dispersion relations DRA and DRS as guides for the real parts. Simultaneously we obtain a value for the subtraction constant K. Determinations of B_I, μ_I and the normalization factor f are made simultaneously. B_I, μ_I are well represented by the simple analytical forms of Eqs. (21) and (22) and Table I. Once the solution for each data set is obtained, the error bars are obtained relaxing the value of each quantity in the fitting code, so that they represent the sensitivity of the χ^2 value, but in general do not include correlations.

Details of the data sets and of the calculation of the analytical representations are given in the figure captions.

A. *pp* data analyzed

1. *Piles of data in four experiments*

Figure 6 shows data from four experiments, [20], [20], [20], and [20], that cover regularly large energy and $|t|$

ranges. In the plots these are called Beznogikh (1973) [20], Kuznetsov (1981) [20], Fajardo (1981) [20] and Burq (1983) [20]. The parameters for the lines are given in Table III. We observe that the representations obtained by Eqs. (2)–(4) are very faithful to the data up to surprisingly large $|t|$ values, namely above $|t| = 0.1$ GeV^2 and up to 0.3 in some cases. The compatibility of different experiments can be noted.

2. *Low energies:* $p_{LAB} = 4$–10 *GeV*

In the very low energy end, there are forward data from Jenni *et al.* [20] at $p_{LAB} = 4.2$, 7 and 10 GeV. At 4.2 and 7 GeV we join Ambats *et al.* [20] at 3.65 and 6 GeV, with factors 0.99 to compensate for the energy dependence.

At $p_{LAB} = 10$ GeV, to exhibit a representative recommendation we join to Jenni *et al.* [20] the data from Beznogikh *et al.* [20] at 9.43 GeV and from Brandenburg *et al.* [20] at 10.4 GeV, with energy adjustment factors, forming a large set with 153 data points.

In all these cases the matching of the experimental sets is very good, and we are then able to find representations of very good quality for $d\sigma/dt$ in elastic pp scattering in all this energy range. The parameters are shown in Table III and the data and representative curves are shown in Fig. 7.

3. *pp scattering in CERN at* $p_{LAB} = 294.4, 313.7$ *and 499.1 GeV*

The energy $p_{LAB} = 294.4$ GeV, with $\sqrt{s} = 23.54$ GeV, of a CERN measurement [20], shown in Fig. 8 is close to the energy $\sqrt{s} = 23.88$ GeV (namely $p_{LAB} = 303$ GeV) of the Fermilab data [20] shown in Fig. 6. The parameters are given in Table III, showing the characteristic feature that ρ crosses zero in this region. The data of the CERN measurements, also at $\sqrt{s} = 24.3$ GeV (thus $p_{LAB} = 313.7$ GeV), and $\sqrt{s} = 30.63$ GeV (thus $p_{LAB} = 499.1$ GeV) are shown together in Fig. 8. All descriptions are of high precision. Other measurements in this energy region, at $p_{LAB} = 303$ and 398 GeV, are included in Fig. 6.

4. *Large* $|t|$: *Behavior beyond the forward range*

The situation at large $|t|$ is shown with Ayres *et al.* data [20] in Fig. 9, where we study the behavior for $|t|$ beyond 0.1 GeV^2. These data do not cover the low-$|t|$ range, and are plotted together with the lines representing the Beznogikh (1973) and Fajardo (1981) data at the corresponding energies. We see a remarkable matching of normalization in the points with smaller $|t|$ and an increasing deviation as $|t|$ increases. We here confirm that the equations for the amplitudes in forward scattering have the validity confirmed up to 0.1 GeV, where regular deviation of the data upwards may start.

Two other plots in the same Fig. 9 show the behavior of data in comparison with the analytic representations for $|t|$
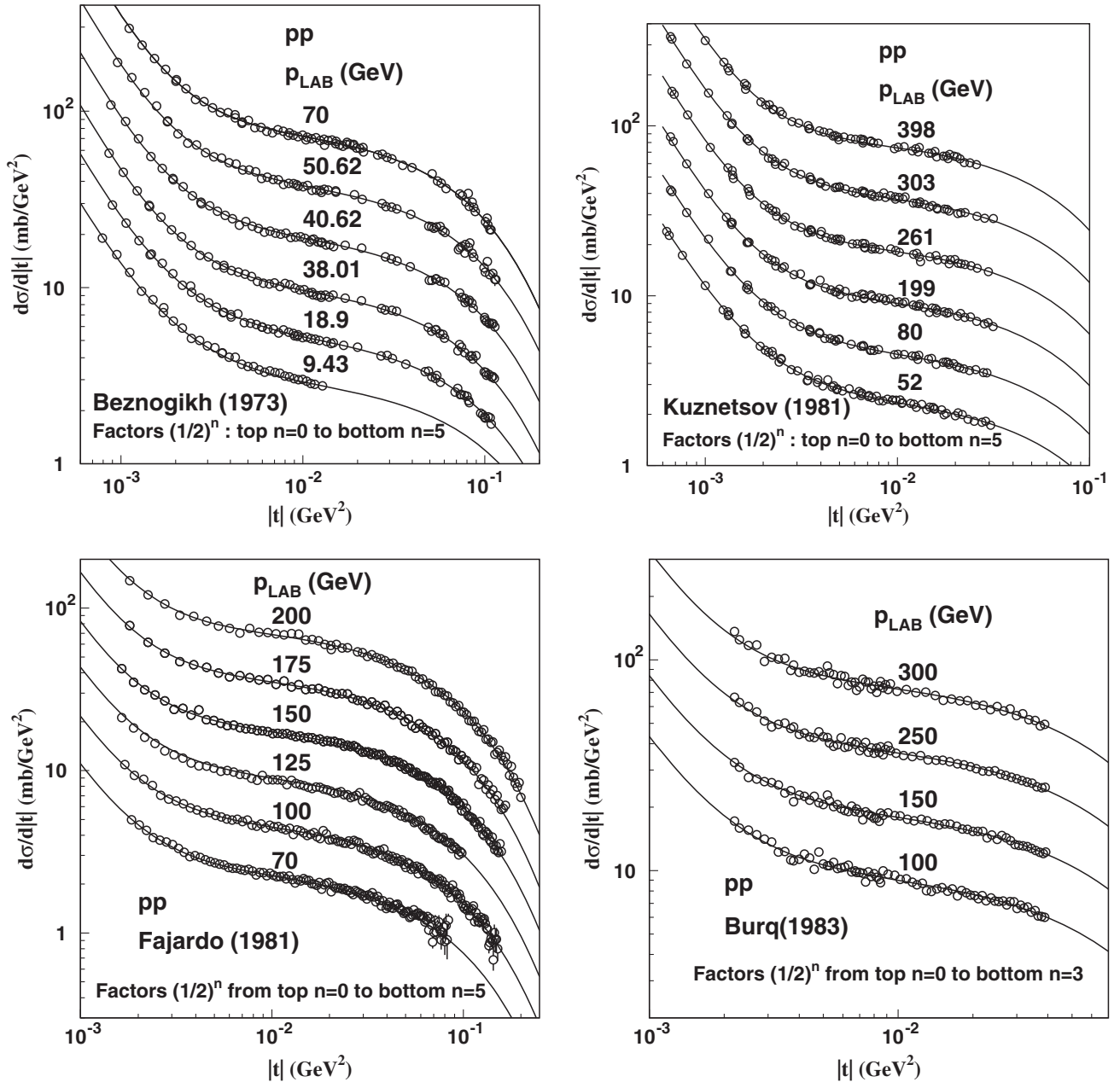
FIG. 6.   Data and suggested representations for pp scattering in the energy range $p_{LAB} = 10$ to 400 GeV, as reported in four different series of measurements [20], [20], [20] and [20]. The data are regular, cover t ranges adequate for determination of forward scattering quantities, and the representation with parameters given in Table III are extremely precise. The compatibility among the four experiments is remarkable. The parameter ρ and the combination $(\rho B_R/2 - \mu_R)$ are in agreement with predictions from dispersion relations for amplitudes DRA and for their derivatives DRS. The framework is explained in the text. The zero of ρ at $p_{LAB} = 277$ GeV that occurs in the energy range of these data is well treated by the representations.

beyond the strict forward region. Details are given in the figure caption.

B. $p\bar{p}$ data analyzed

At low energies, the analysis of the $p\bar{p}$ forward scattering data is particularly difficult, because ρ is very small, and changes sign for $p_{LAB} = 117$ GeV ($\sqrt{s}$ near 12 GeV).

1. $p\bar{p}$ in the range $p_{LAB} = 4.2$–10.0

The range is $\sqrt{s} = 3.14$–4.54 GeV in $p\bar{p}$ scattering is difficult to treat, because ρ is very small, possibly passing through zero in this range. In Fig. 10 we show data collected at the energies $p_{LAB} = 4.2$, 6.0, 8.0 and 10.0 GeV corresponding to measurements of Jenni et al. [20] with $|t|$ starting at about 10^{-3} GeV^2. These data are not smooth and do not cover a wide t range, so that they are
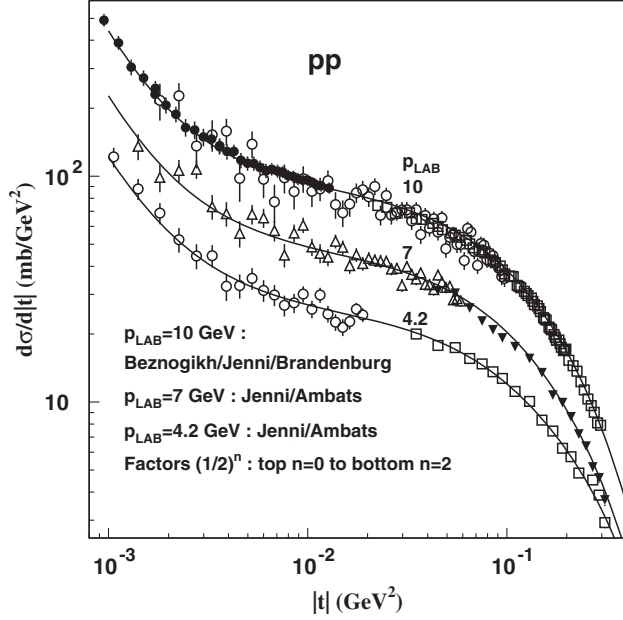
FIG. 7. Data for pp scattering in the low energy end, with Jenni points [20] at 4.2, 7 and 10 GeV in the forward range. At 4.2 and 7 GeV, data from Ambats *et al.* [20] at 3.65 and 6 GeV respectively with large $|t|$ are incorporated in the sets, after multiplication by the same factor 0.99 accounting for the energy dependence. At $p_{LAB} = 10$ we plot together in a single set data from three different experiments [20], [20], and [20] at 9.43, 10 and 10.4 GeV respectively, introducing conversion factor 0.97 at 10.24 GeV to account for energy dependence. For 9.43 the factor is nearly 1, and is ignored. In all cases the connection of the data sets is remarkable. The data at 9.43 GeV are also plotted in a pile of the same experiment [20] in Fig. 6. The parameters are given in Table III.
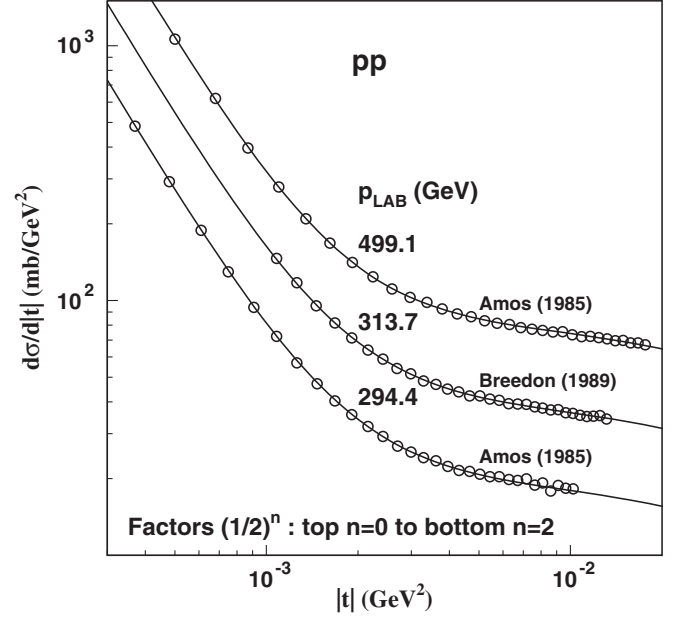

FIG. 8. CERN data [20] and [20] in the higher energy part of our analysis with parameters given in Table III. Other measurements in the same region are shown in Fig. 6.

combined with other data in the range to build sufficient sets. The assemblage is shown in plots, with the lines representing the results of the analysis, with parameters given in Table IV.

At 4.2 GeV the combination is made with the $p_{LAB} = 5$ GeV data of Ambats *et al.* [20], multiplied by 1.06 to account for the energy dependence. At 6 GeV the merging is with Braun *et al.* [20] at $p_{LAB} = 5.7$ GeV (multiplied by the energy dependence factor 0.98). At 8 GeV the combination is made with Russ *et al.* [20] at the same energy. At 10 GeV the set is completed with data at 10.4 GeV from Brandenburg *et al.* [20] with a factor 1.0117. The energy factors are based on the squared ratio of the total cross section given by the parametrized σ input. We thus obtain values for parameters that give reliable proposals in a region of energies that is very difficult, because ρ is very small. Our representations with Eqs. (2)–(4) and parameters given in Table IV give correct descriptions of these data. The dispersion relations predictions for ρ and for the derivative combination $\rho B_R/2 - \mu_R$ are satisfied.

2. $p\bar{p}$ data in the mid-$|t|$ range for $p_{LAB} = 16$–50 GeV

The data in Fig. 11, with $p_{LAB} = 16$–50 GeV, cover only the mid-$|t|$ range. It is interesting to observe in general that the representation of data using the forward scattering expression for $d\sigma/dt$, in principle is only valid up to $|t| = 0.1$ GeV^2, in many cases remain good up to 0.5.

According to Ayres [20], Akerlof data [20], also at mid-$|t|$, have a normalization problem, and then are not included in our report in Table IV.

3. $p\bar{p}$ in the range $p_{LAB} = 70$–200 GeV

This is a sensitive range for the determination of ρ, due to the change of sign. In $p\bar{p}$ ρ is small and negative at low energies up to about $p_{LAB} = 116$ GeV. The data by Ayres [20] at $p_{LAB} = 50, 70, 100, 140$ and 175 GeV are regular and with small error bars but are restricted to $|t|$ values that are not small enough for determination of forward scattering parameters, and we then form combinations with other sets of data, as shown in Fig. 12. At $p_{LAB} = 70$ and 175 GeV these data can be combined with the data from Fajardo *et al.* [20] to produce sets that cover both small and mid-$|t|$ values. Some parts of Fajardo data [20] in the higher $|t|$ part are excluded, giving place to Ayres data [20], which are more regular. It is remarkable that the data from the two experiments match very well, and a common solution seems to be adequate. At $p_{LAB} = 70$ GeV the data give ρ compatible with zero, and in Table IV we choose the value given by the DRA prediction. This is a choice, and the value and sign have the corresponding uncertainty.
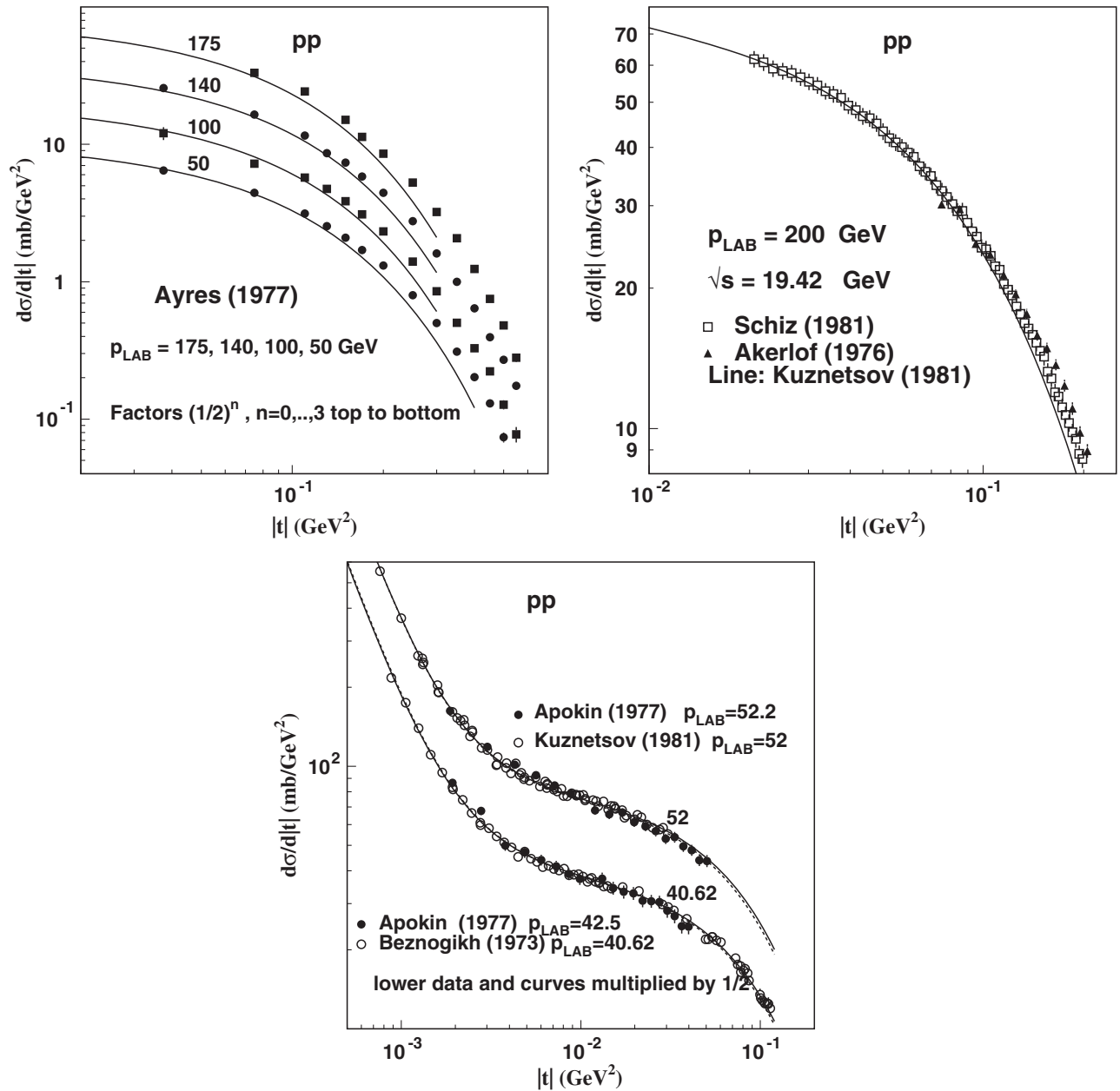
FIG. 9.   Deviations for large $|t|$. In the first plot (a) (lhs at top) we show data for $|t|$ in the frontier of the forward region from Ayres *et al.* [20]. The lines are NOT obtained with these data, but rather are taken from the description of the forward range in Fig. 6, with the parameters as given in Table III, at the corresponding energies. For the 140 GeV data there is no corresponding low-$|t|$ experiment, and we use the line for 150 GeV [20]. The matching of points of lowest $|t|$ at each energy is impressive, showing that different experiments succeed in the normalization of their data. At all energies there is a progressive detachment between data and predicted curves starting at, say, 0.1 GeV, showing clearly that these data by themselves cannot be used for determinations. In the second plot (b) (rhs at top) we show the connection between the solution at 199 GeV [20] and the forward part (up to 0.2 GeV^2) of data by Schiz *et al.* [20] that starts at $|t| = 0.02$ GeV^2. The solid line represents the curve for Kuznetsov data at 199 GeV in Fig. 6 with parameters given in Table III. The agreement of Schiz data with the curve up to $|t| \approx 0.1$ GeV^2 is remarkable but it seems that improvement could be obtained with normalization. We observe that for higher $|t|$ there appears a displacement between data and the curve, exhibiting again the limitation for the use of the forward amplitudes. For illustrative purpose, we show together Akerlof *et al.* points [20] added to the 200 GeV plot, demonstrating that they should not be considered in good agreement (notice that the scale is very tight), presenting strong displacement as $|t|$ increases. In the third plot (c) (bottom) we show Apokin *et al.* data [20] at $p_{\mathrm{LAB}} = 42.5$ and 52.2 GeV, covering smaller $|t|$ ranges, inserted together with Beznogikh [20] and Kuznetsov [20] data respectively. We observe compatibility (the 42.5 data are corrected with factor 1.02 in the plot, to reduce to energy 40.62 GeV). The lines of the solution for Apokin [20] are shown in dashed form, while the Beznogikh and Kuznetsov lines are solid. There is reasonable compatibility, but it is clear that the measurements reaching smaller $|t|$ values are more qualified for parameter determination.
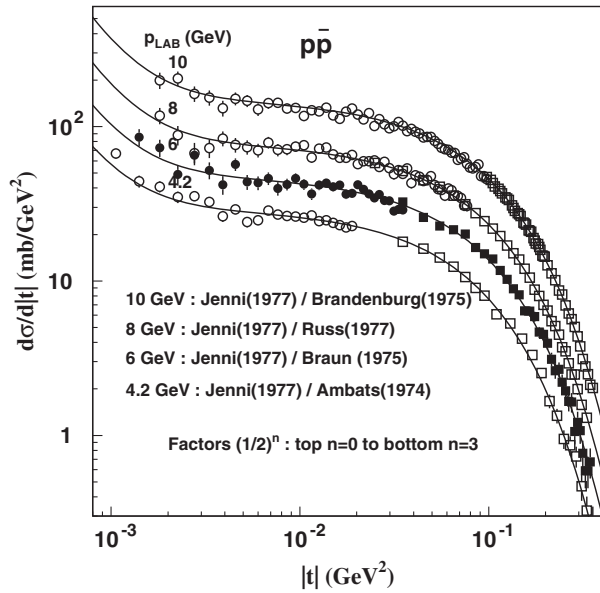
FIG. 10. Low energy end. At 4.2 GeV, data from Jenni *et al.* [20] together with data from Ambats [20] at 5 GeV (multiplied by 1.06 to account for energy dependence). Data from Jenni *et al.* [20] at 6 GeV, and from Braun *et al.* [20] for $p_{LAB} = 5.7$ GeV (multiplied by 0.98). Data from Jenni *et al.* [20] and from Russ *et al.* [20] at 8 GeV, and data from Jenni *et al.* [20] at 10 GeV and from Brandenburg *et al.* [20] at 10.4 GeV (multiplied by 1.0117). Visually (up to $|t| \approx$ GeV^2) and in the calculations the matching of data is impressive. Parameter values for each line are given in Table IV.
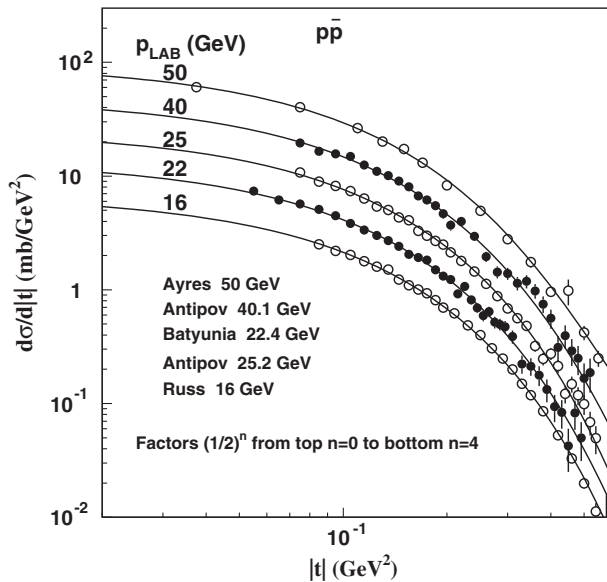
FIG. 11. Mid *t* Range. Data with measurements at mid$|t|$ only. Data from Russ *et al.* [20], Antipov *et al.* [20], Ayres *et al.* [20], Batyunia *et al.* [20] at $p_{LAB} = 16, 22.4, 25.2, 40.1$ and 50 GeV, described with the parameter values of Table IV, presenting regular energy dependence. It is remarkable that the lines reproduce well the data up to 0.5 GeV^2. Notice that the original Antipov data at 40.1 GeV have been remeasured and published with changes in 1977 [20], and a factor 1.15 is used to adjust the old to the new published data.

We observe in Table IV that at $p_{LAB} = 125$ GeV, ρ is positive, confirming the change of sign that occurs at $p_{LAB} = 117$ GeV.

At all energies of the range, the suggested solutions in Table IV give very good descriptions, as indicated by the low χ^2 values. We are able to follow the DRA and DRS predictions for the value of the amplitude and for its derivative at the origin. It is interesting to observe that often the representation of data using the forward scattering expression for $d\sigma/dt$, in principle only valid up to $|t| = 0.1$ GeV^2, in many cases remains good up to 0.2 GeV^2. This is seen also in both Figs. 11 and 12.

We observe that in this range the numbers reported in experimental papers for the ρ parameter are very irregular and with contradictions.

4. $p\bar{p}$ in the range $p_{LAB} = 300$–500 GeV

At the high energies $\sqrt{s} = 24.3$ and 30.4 GeV there are data from CERN ISR, with good precision in forward scattering measurements. The treatment of these data with our inputs is reproduced in Fig. 13.
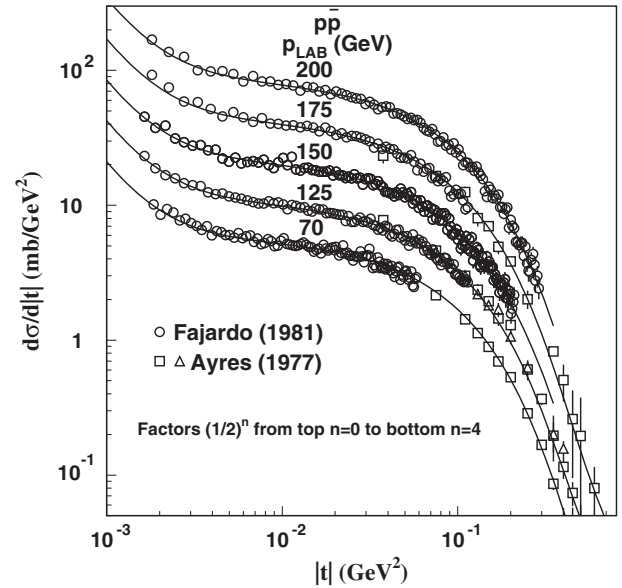

FIG. 12. Data from Fajardo *et al.* [20], and from Ayres *et al.* [20] described by the parameters given in Table IV. At 125 GeV the solution refers only to Fajardo; the Ayres points at 100 and 140 GeV are not fitted, and only marked together with the 125 GeV line of Fajardo. The Jenni data are restricted to a range of large $|t|$ values, with difficulty for determination of parameters, but are important to confirm the data of Fajardo. It is interesting to observe that $d\sigma/dt$ for large $|t|$ is not very sensitive to the energy. At 70 and 175 GeV, there are measurements for both Jenni and Fajard, and then the respective data are merged to form joint sets for the unified determination of parameters that are given in Table IV. At $p_{LAB} = 150$ and 200 GeV the points are only from Fajardo.
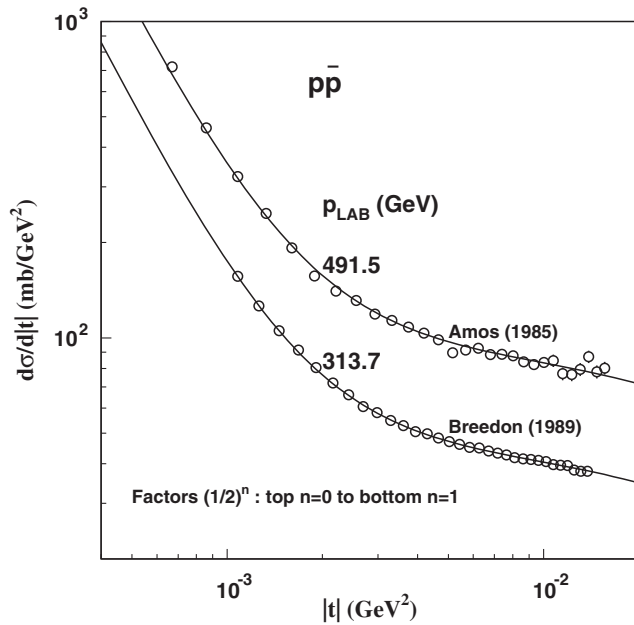
FIG. 13. Data from Breedon et al. [20] and from Amos et al. [20] described by the parameters given in Table IV. The numerical values of $d\sigma/dt$ for $p_{\text{LAB}} = 313.7$ GeV ($\sqrt{s} = 24.3$ GeV) are available from the thesis of author Breedon [20], and also in the CERN Library.

IV. CONCLUDING REMARKS

In this paper we propose a revision of the existing information on forward parameters in pp and $p\bar{p}$ scattering, giving coherent and precise description of all elastic data in the energy range from $p_{\text{LAB}} \approx 4$ to 500 GeV, namely $\sqrt{s} \approx 3$ to 30 GeV.

We treat the fundamental problem of the identification of the real and imaginary parts of the complex amplitude in $d\sigma/dt$, using Eqs. (3) and (4) and exact solutions of dispersion relations for amplitudes (DRA) and for slopes (DRS). The Coulomb interference is included with correct expression for the phase in Eq. (2), which depends on the actual analytical form of the real amplitude, and is studied in Appendix A. We do not perform open fittings, but rather rationalize descriptions, in an interplay between data and mathematical representations, building a bridge for the construction of full dynamical models.

The analysis of the $d\sigma/dt$ data leads to the parameter values presented in Tables III and IV, given in Sec. III. Determination of parameters is guided by dispersion relations and criteria of regularity in the energy dependence, in general achieving low χ^2 values, with visual performances exhibited in plots in Sec. III. The description is coherent and theoretically respectable and formally simple.

A global analysis in the low energy range must be restricted to the forward range, because there are not enough data for a full-t study of the amplitudes. Since the imaginary amplitudes dominate at small $|t|$, our

precision work has particular importance as an investigation of the structure of the real parts. At low energies the use of dispersion relations requires the use of exact solutions for principal value integrals, as we prove in Appendix B.

For a precise treatment of the data, the t dependence of the amplitudes cannot be limited to exponential forms. It is known that the imaginary part must point to a zero because there is a dip in $d\sigma/dt$ shown when data have more extended $|t|$. Also the real part must show a zero when ρ is positive, determined by Martin's theorem [21]. We we thus are led to the amplitudes written in Eqs. (3) and (4). To deal with this complexity without ambiguities in the analysis of data, we make use of the dispersion relations for slopes (DRS), which determine the derivatives of the real part when the derivatives of the imaginary parts are given as a function of the energy.

The proposals for σ, B_I and μ_I (for pp and for $p\bar{p}$) in Eqs. (19), (21) and ((22), obtained from the data, are basic in our work as inputs for DRA and DRS. Figure 2 shows that the analytical forms have correct extensions up to the very distant LHC energies.

Starting with the unitarized form for $\sigma(x)$ originated in Pomeron/Reggeon phenomenology [22], and complemented with the $|t|$ structure of the imaginary part, the description of the $d\sigma/dt$ data shows that all information in elastic scattering at low energies can be represented by simple expressions for the amplitudes. We believe that the simple forms of energy dependence are a consequence of the very complex gluonic dynamics of QCD. Local effects that may be meaningful microscopically are absorbed in the complexity and do not become visible in elastic data.

In Appendix C it is shown that the log-squared form of the total cross section in Eq. (19) is shown to be equivalent to a simple-pole-Pomeron/Reggeon form, with powers instead of logarithms, and thus without limitation for the analytical solutions of PV integrals.

As an important test for the amplitudes, Fig. 3 in Sec. II shows that the integrated elastic cross section σ^{elastic} very well reproduces the data at higher energies (ISR, Fermilab, LHC) [4,5]. The ratio $\sigma^{\text{elastic}}/\sigma^{\text{total}}$ is small, corresponding to a large fraction of diffractive and inelastic contributions, which have not been measured in the low energy range and are not in our scope. The single and double diffractive processes, measured at ISR/CERN, Fermilab and LHC [4,5], are theoretically studied in microscopic terms based on multi-Pomeron/Reggeon ideas [8] and on gluonic dynamics of the color glass condensate [9].

The analysis of the $p\bar{p}$ data at low energies is particularly delicate, because ρ is very small and has change of sign. Most $p\bar{p}$ data do not cover $|t|$ ranges sufficient for determination of the amplitude parameters without support of DRA, DRS and search for regular energy dependence. We include as much $p\bar{p}$ information as possible, forming combinations of different experiments at nearby energies to have sets suitable for analysis, arriving at reliable solutions.

Figure 4 shows that ρ and the derivative $D_R = \rho B_R / 2 - \mu_R$ follow DRA and DRS predictions. Figure 5 shows the proposed decomposition of D_R, with μ_R given by Eqs. (50) and (51), and shows the calculated B_R, compared to values obtained from the data. Everything seems satisfactory, including the behavior as high energies, where these quantities appear [7,10]. Negative μ_R predicts the zero of the real amplitude in a region where ρ is positive, as at high energies [21], with the real zero approaching $|t| = 0$ with increasing energy. Of course alternative solutions can be obtained for μ_R and B_R, maintaining the combination Eq. (11) as fixed by DRS.

This extensive work is an effort to place order in the multitude of determinations of pp and $p\bar{p}$ forward scattering parameters at low energies. The treatment is as simple as possible, without relation to any specific model based on microscopic ingredients, and identifies the real and imaginary parts of the complex elastic amplitude. We hope it can be considered as necessary and useful.

ACKNOWLEDGMENTS

APPENDIX A: COULOMB PHASE

We here present the Coulomb interference phase ϕ used in the phenomenology. This phase was studied by several authors [16].

The expression for the phase depends on the analytical structure of the real and imaginary parts of the nuclear amplitude and also on the Coulomb amplitude and electromagnetic form factor. The real and imaginary nuclear amplitudes are given by Eqs. (3) and (4) respectively and the Coulomb amplitude is given by Eq. (6) with the proton form factor (7). To simplify calculations, we may alternatively use the exponential representation for the form factor

$$f(t) = e^{2t/\Lambda^2}, \tag{A1}$$

with $\Lambda^2 = 0.71 \text{ GeV}^2$, trusting that differences in results for the phases with different form factors are unimportant, as confirmed by Cahn [16].

The Coulomb-nuclear-interference amplitude is given by

$$F^{N+C}(s,t) = F^C(s,t)e^{i\alpha\phi} + F^N(s,t) \tag{A2}$$

with normalization defined by

$$\sigma = \frac{4\pi}{s} \text{Im} F^N(t=0), \qquad \frac{d\sigma}{dt} = \frac{\pi}{s^2}|F|^2. \tag{A3}$$

The correspondence between the dimensionless nuclear amplitude F^N and the phenomenological T^N is given by

$$T^N(s,t) = \frac{\sqrt{\pi}}{(\hbar c)^2} \frac{F^N(s,t)}{s}. \tag{A4}$$

We start from the expression for the phase

$$\phi(s,t) = \mp \int_0^\infty dt' \ln\left(\frac{t'}{t}\right) \frac{d}{dt'}\left[f^2(t')\frac{F_N(s,t')}{F_N(s,0)}\right], \tag{A5}$$

with the signs $\mp$ corresponding to the $pp/p\bar{p}$ systems.

As a generalization with respect to Cahn's calculation, we take for the nuclear amplitude the same expressions in Eqs. (3) and (4). Then we need to evaluate integrals

$$
\begin{aligned}
H_k(t,b_\beta) &= \int_0^{-\infty} dt' \ln\left(\frac{t'}{t}\right) \frac{d}{dt'}[t'^k e^{4t'/\Lambda^2} e^{B_\beta t'/2}] \\
&= \int_0^{-\infty} dt' \ln\left(\frac{t'}{t}\right) \frac{d}{dt'}[t'^k e^{b_\beta t'}],
\end{aligned} \tag{A6}
$$

where we have used the definition

$$b_\beta = \frac{4}{\Lambda^2} + \frac{B_\beta}{2} \tag{A7}$$

with $\beta = R, I$.

The results of the integrations ($k = 0, 1$) are

$$H_0 = \gamma + \log(-b_\beta t), \qquad H_1 = \frac{1}{b_\beta}, \tag{A8}$$

where $\gamma = 0.5772$ is the Euler Gamma constant. The phase is then written

$$
\begin{aligned}
\phi(s,t) = \mp \frac{1}{\rho+i}\Bigg\{ &\left[-\frac{\mu_R}{b_R} + \rho(\gamma + \log(-b_R t))\right] \\
&+ i\left[-\frac{\mu_I}{b_I} + \gamma + \log(-b_I t)\right]\Bigg\},
\end{aligned} \tag{A9}
$$

with real and imaginary parts respectively

$$
\begin{aligned}
\phi_R(t) = \mp \Bigg\{ &\frac{1}{1+\rho^2}\left[\left(-\frac{\mu_I}{b_I} + \log(b_I)\right)\right. \\
&\left.+ \rho\left(-\frac{\mu_R}{b_R} + \rho\log(b_R)\right)\right] + \gamma + \log(-t)\Bigg\}
\end{aligned} \tag{A10}
$$

and

$$
\begin{aligned}
\phi_I(t) = \mp \frac{1}{1+\rho^2}\Bigg\{ &\rho\left(-\frac{\mu_I}{b_I} + \log(b_I)\right) \\
&- \left(-\frac{\mu_R}{b_R} + \rho\log(b_R)\right)\Bigg\}.
\end{aligned} \tag{A11}
$$

Equations (A10) and (A11) are our final results for the phase calculated with form factors, in a generalization of

the work by Cahn [16], assuming more complete structures for the real and imaginary parts of the scattering amplitude. It may be of practical usefulness to define

$$C_R = -\frac{\mu_R}{b_R} + \rho \log(b_R) \qquad (A12)$$

and

$$C_I = -\frac{\mu_I}{b_I} + \log(b_I) \qquad (A13)$$

and then write

$$\phi_R(t) = \mp \left[\frac{1}{1+\rho^2}[C_I + \rho C_R] + \gamma + \log(-t) \right] \qquad (A14)$$

and

$$\phi_I(t) = \mp \frac{1}{1+\rho^2}[\rho C_I - C_R]. \qquad (A15)$$

It must be observed that in these expressions b_R, b_I and $-t$ have compatible units, as GeV^{-2} and GeV^2. The result is simple: in the real part the t dependence is purely linear in $\log(-t)$, the imaginary part is very small constant, and there is no explicit energy dependence.

In the simplified case $\mu_R = \mu_I = 0$, $B_R = B_I = B$,

$$b_R = b_I = b = \frac{4}{\Lambda^2} + \frac{B}{2}$$

we obtain Cahn's original form.

APPENDIX B: DISPERSION RELATIONS IN EXPANDED FORMS

1. Dispersion relations for amplitudes

Introduction of the inputs of $\sigma(x)$, $B_I(x)$, $\mu_I(x)$ given in Eqs. (19), (21), and (22), DRA and DRS become the sum of terms with principal value integrals, all of the general form

$$I(n, \lambda, x) = \mathbf{P} \int_1^{+\infty} \frac{x'^\lambda \log^n(x')}{x'^2 - x^2} dx', \qquad (B1)$$

belonging to a family of integrals that can be solved analytically in terms of Lerch's transcendents Φ [14] with the form

$$I(n, \lambda, x) = \frac{\pi}{2x} \frac{\partial^n}{\partial \lambda^n}\left[x^\lambda \tan\left(\frac{\pi}{2}\lambda\right) \right]$$
$$+ \frac{(-1)^n n!}{2^{n+1} x^2} \Phi\left(\frac{1}{x^2}, n+1, \frac{1+\lambda}{2}\right). \qquad (B2)$$

Collecting terms, we have for the even and odd parts of DRA

$$\text{Re}F_+(x, 0) = K + \frac{4m^2 x^2}{\pi}[I(0, 0, x)(P + H\log^2 x_0)$$
$$+ I(1, 0, x)(-2H \log x_0)$$
$$+ I(2, 0, x)H + I(0, -\eta_1, x)R_1 x_0^{\eta_1}] \qquad (B3)$$

and

$$\text{Re}F_-(x, 0) = \frac{4m^2 x}{\pi} I(0, 1 - \eta_2, x)R_2 x_0^{\eta_2}. \qquad (B4)$$

Equations (B3) and (B4) lead to the real parts of the complex amplitude for pp and $p\bar{p}$ elastic scattering, and then we have predictions for the parameters ρ (pp, $p\bar{p}$).

Using the practical truncated expression for the transcendents (up to first order in $1/x$) we have for the even combination

$$\frac{1}{2}[(\sigma\rho)(p\bar{p}) + (\sigma\rho)(pp)] = \frac{1}{2m^2 x}\text{Re}F_+(x, 0)$$
$$\approx T_1(x) + T_2(x) + T_3(x), \qquad (B5)$$

with

$$T_1(x) = H\pi \log\left(\frac{x}{x_0}\right), \qquad (B6)$$

$$T_2(x) = \frac{K}{2m^2 x}$$
$$+ \frac{2}{\pi x}(P + H[\log^2(x_0) + 2\log(x_0) + 2]), \qquad (B7)$$

$$T_3(x) = R_1 x_0^{\eta_1}\left[-x^{-\eta_1} \tan\left(\frac{\pi\eta_1}{2}\right) + \frac{1}{x}\frac{2/\pi}{1-\eta_1} \right], \qquad (B8)$$

and for the odd part

$$\frac{1}{2}[(\sigma\rho)(p\bar{p}) - (\sigma\rho)(pp)]$$
$$= \frac{1}{2m^2 x}\text{Re}F_-(x, 0)$$
$$\approx R_2 x_0^{\eta_2}\left[x^{-\eta_2} \cot\left(\frac{\pi\eta_2}{2}\right) + \frac{1}{x^2}\frac{2/\pi}{2-\eta_2} \right]. \qquad (B9)$$

Additional terms are of order $\mathcal{O}(x^{-4})$.

Using the parameter values for P, H, R_1, R_2 in Table I and with $K = -310$, the calculated ρ values are plotted in Fig. 14. To demonstrate the importance of the calculation with the exact solutions for the PV integrals, we plot in the figure the ρ values obtained with the above expressions (namely first order in the transcendents) and in zero order (very large x, meaning the above expressions without the last terms with $2/\pi/1 - \eta_1$ and $2/\pi/2 - \eta_2$). From the figure we observe the importance of the improved solutions at low energies.
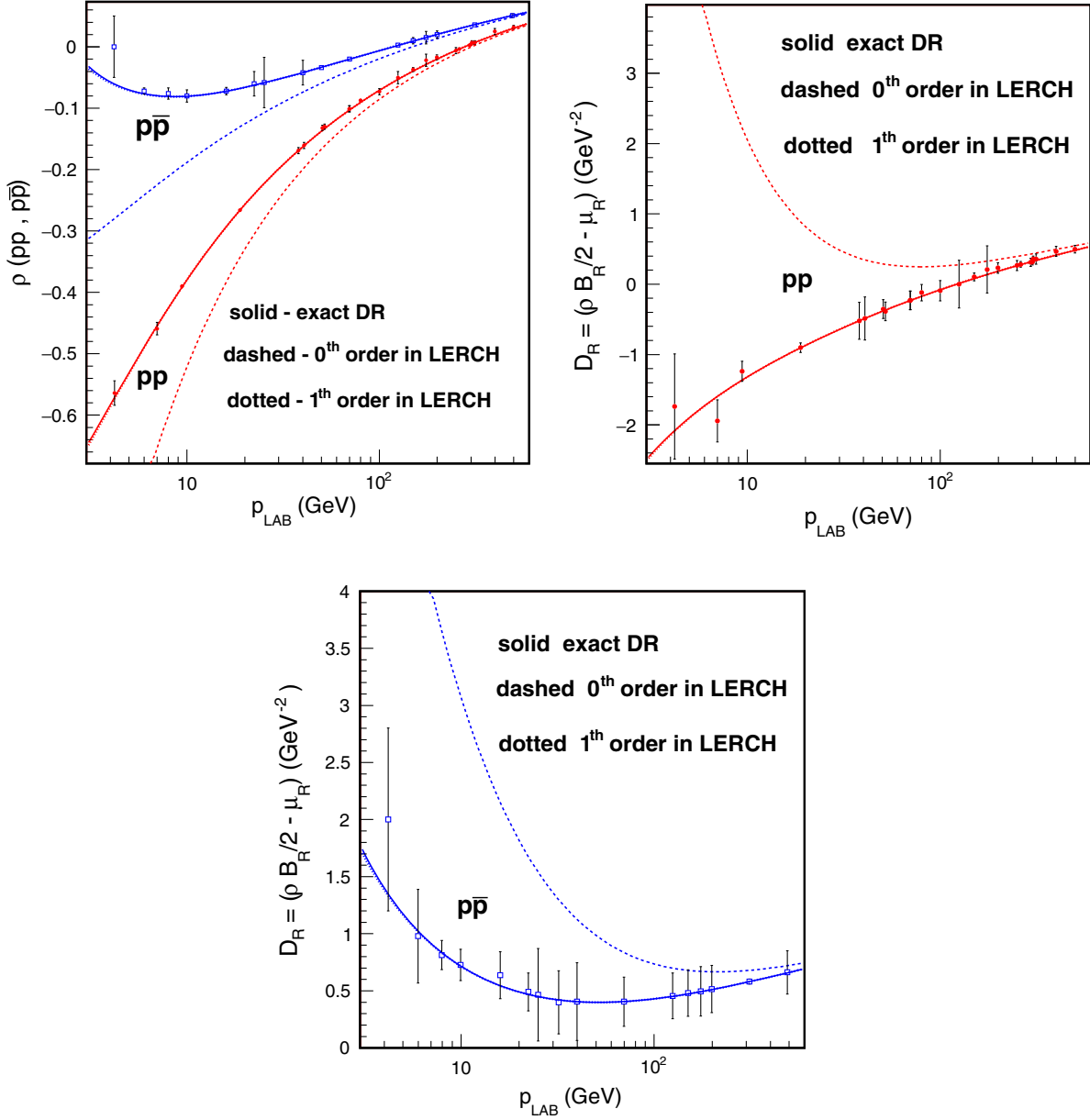
FIG. 14. Demonstration of the importance of calculations with improved solutions for the PV integrals. (a) ρ parameters. (b) and (c) Energy dependence of the derivatives of the real amplitudes at $t = 0$. The lines are fully predicted by the dispersion relations for the amplitudes (that give ρ for pp and $p\bar{p}$) and by dispersion relations for slopes DRS (that give $D_R = \rho B_R/2 - \mu_R$ for pp and $p\bar{p}$).

2. Dispersion relations for slopes

In the same way, the DRS terms are collected in terms of the standard integrals. We obtain for the even part

$$
\begin{aligned}
\frac{\partial \mathrm{Re} F_+(x,t)}{\partial t}\bigg|_{t=0} = \frac{2m^2 x^2}{\pi} \{ & I(0,0,x)(P + H\log^2 x_0)b_0' + I(1,0,x)[(-2H\log x_0)b_0' + (P + H\log^2 x_0)b_1'] \\
& + I(2,0,x)[Hb_0' - 2H\log x_0 b_1' + (P + H\log^2 x_0)b_2] + I(3,0,x)[-2H\log x_0 b_2 + Hb_1'] + I(4,0,x)Hb_2 \\
& + R_1 x_0^{\eta_1}(I(0,-\eta_1,x)b_0' + I(1,-\eta_1,x)b_1' + I(2,-\eta_1,x)b_2 + I(0,-\eta_1-\eta_3,x)b_3) \\
& + R_2 x_0^{\eta_2} I(0,-\eta_2-\eta_4,x)b_4 + [(P + H\log^2 x_0)I(0,-\eta_3,x) \\
& - 2H\log x_0 I(1,-\eta_3,x) + HI(2,-\eta_3,x)]b_3 \},
\end{aligned}
\tag{B10}
$$

and for the odd part

$$\left.\frac{\partial \mathrm{Re}F_-(x,t)}{\partial t}\right|_{t=0} = \frac{2m^2x}{\pi}\{R_2x_0^{\eta_2}(I(0,1-\eta_2,x)b_0' + I(1,1-\eta_2,x)b_1' + I(2,1-\eta_2,x)b_2 + I(0,1-\eta_2-\eta_3,x)b_3)$$

$$+ ((P + H\log^2x_0)I(0,1-\eta_4,x) - 2H\log x_0 I(1,1-\eta_4,x) + HI(2,1-\eta_4,x)$$

$$+ R_1x_0^{\eta_1}I(0,1-\eta_1-\eta_4,x))b_4\}. \tag{B11}$$

We recall Eq. (48) with the definitions of b_0' and b_1'.

Explicit expressions for the derivative DR including only the first terms of the expansions of the transcendents are

$$\frac{1}{2m^2x}\left.\frac{\partial \mathrm{Re}F_+(x,t)}{\partial t}\right|_{t=0} = \frac{1}{2}\{\sigma_{p\bar{p}}[\rho B_R/2 - \mu_R](p\bar{p}) + \sigma_{pp}[\rho B_R/2 - \mu_R](pp)\}$$

$$= \frac{1}{\pi}[(P + H\log^2x_0)G_1(x) + HG_2(x) + R_1G_3(x) + R_2G_4(x)], \tag{B12}$$

where

$$G_1(x) \equiv \frac{b_0' - b_1' + 2b_2}{x} + \frac{b_1'\pi^2}{4} + \frac{b_2\pi^2}{2}\log x + b_3\left(-\frac{\pi}{2}x^{-\eta_3}\tan\left(\frac{\pi\eta_3}{2}\right) + \frac{1}{x}\frac{1}{1-\eta_3}\right), \tag{B13}$$

$$G_2(x) \equiv \left[\frac{\pi^2}{4}\left(3\log^2x + \frac{\pi^2}{2}\right) - \frac{6}{x}\right](b_1' - 2b_2\log x_0) - 2b_0'\log x_0\left(\frac{\pi^2}{4} - \frac{1}{x}\right)$$

$$+ (b_0' - 2b_1'\log x_0)\left(\frac{\pi^2}{2}\log x + \frac{2}{x}\right) + b_2\left[\pi^2\log x\left(\log^2x + \frac{\pi^2}{2}\right) + \frac{24}{x}\right]$$

$$- \pi b_3 x^{-\eta_3}\left[\log x\tan\left(\frac{\pi\eta_3}{2}\right)\left(-\log x_0 + \frac{1}{2}\log x\right) - \frac{\pi}{2}\sec^2\left(\frac{\pi\eta_3}{2}\right)\left(\log\left(\frac{x}{x_0}\right) - \frac{\pi}{2}\tan\left(\frac{\pi\eta_3}{2}\right)\right)\right]$$

$$+ \frac{2b_3}{x(1-\eta_3)^2}\left(\log x_0 + \frac{1}{1-\eta_3}\right), \tag{B14}$$

$$G_3(x) \equiv x_0^{\eta_1}\left\{b_0'\left[\frac{\pi}{2}x^{-\eta_1}\tan\left(-\frac{\pi\eta_1}{2}\right) + \frac{1}{x}\frac{1}{1-\eta_1}\right] + b_1'\frac{\pi}{2}x^{-\eta_1}\left[\frac{\pi}{2}\sec^2\left(\frac{\pi\eta_1}{2}\right) - \tan\left(\frac{\pi\eta_1}{2}\right)\log x\right]\right.$$

$$- b_2\frac{\pi^2}{2}x^{-\eta_1}\left[\sec^2\left(\frac{\pi\eta_1}{2}\right)\left(\frac{\pi}{2}\tan\left(\frac{\pi\eta_1}{2}\right) - \log x\right) + \frac{1}{\pi}\tan\left(\frac{\pi\eta_1}{2}\right)\log^2x\right]$$

$$\left.+ b_3\left[-\frac{\pi}{2}x^{-\eta_1-\eta_3}\tan\left(\frac{\pi(\eta_1+\eta_3)}{2}\right) + \frac{1}{x}\frac{1}{1-\eta_1-\eta_3}\right] + \frac{1}{x}\frac{1}{(1-\eta_1)^2}\left(-b_1' + \frac{2b_2}{(1-\eta_1)}\right)\right\}, \tag{B15}$$

$$G_4(x) \equiv x_0^{\eta_2}b_4\left[-\frac{\pi}{2}x^{-\eta_2-\eta_4}\tan\left(\frac{\pi(\eta_2+\eta_4)}{2}\right) + \frac{1}{x}\frac{1}{1-\eta_2-\eta_4}\right]. \tag{B16}$$

For the odd combination we have

$$\frac{1}{2m^2x}\left.\frac{\partial \mathrm{Re}F_-(x,t)}{\partial t}\right|_{t=0} = \frac{1}{2}\{\sigma_{p\bar{p}}[\rho B_R/2 - \mu_R](p\bar{p}) - \sigma_{pp}[\rho B_R/2 - \mu_R](pp)\}$$

$$= \frac{1}{\pi}[(P + H\log^2x_0)F_1(x) + HF_2(x) + R_1F_3(x) + R_2F_4(x)], \tag{B17}$$

where

$$F_1(x) \equiv b_4\left(\frac{\pi}{2}x^{-\eta_4}\cot\left(\frac{\pi\eta_2}{2}\right) + \frac{1}{x^2}\frac{1}{2-\eta_4}\right), \tag{B18}$$

$$F_2(x) \equiv b_4 \left\{ \frac{\pi}{2} x^{-\eta_4} \left[\pi \csc^2\left(\frac{\pi\eta_4}{2}\right) \left(\log\left(\frac{x}{x_0}\right) + \frac{\pi}{2}\cot\left(\frac{\pi\eta_4}{2}\right) \right) \right. \right.$$
$$\left. + \cot\left(\frac{\pi\eta_4}{2}\right) \log x (-2\log x_0 + \log x) \right]$$
$$\left. + \frac{2}{x^2} \frac{1}{(2-\eta_4)^2} \left(\log x_0 + \frac{1}{2-\eta_4} \right) \right\}, \tag{B19}$$

$$F_3(x) \equiv b_4 x_0^{\eta_1} \left[\frac{\pi}{2} x^{-\eta_1-\eta_4} \cot\left(\frac{\pi}{2}(\eta_1+\eta_4)\right) + \frac{1}{x^2} \frac{1}{2-\eta_1-\eta_3} \right], \tag{B20}$$

$$F_4(x) \equiv x_0^{\eta_2} \left\{ \frac{\pi}{2} x^{-\eta_2} \left[\cot\left(\frac{\pi\eta_2}{2}\right)(b_0' + b_1'\log x + b_2\log^2 x) \right. \right.$$
$$+ \frac{\pi}{2}\csc^2\left(\frac{\pi\eta_2}{2}\right)\left(b_1' + \pi\cot\left(\frac{\pi\eta_2}{2}\right)b_2 + 2\log x b_2 \right)$$
$$\left. + x^{-\eta_3}\cot\left(\frac{\pi}{2}(\eta_2+\eta_3)\right)b_3 \right]$$
$$\left. + \frac{1}{x^2}\frac{1}{2-\eta_3}\left[b_0' - \frac{b_1'}{2-\eta_2} + \frac{2b_2}{(2-\eta_2)^2} + \frac{(2-\eta_2)b_3}{2-\eta_2-\eta_3} \right] \right\}. \tag{B21}$$

In Fig. 14 the quantities D_R for pp and $p\bar{p}$ are plotted using the above expressions (first order in the transcendents) and the calculations where Φ is ignored.

These equations, here called dispersion relations for amplitudes (DRA) and dispersion relations for slopes (DRS), control quantities observed in forward scattering and should be used as basic information for phenomenological and theoretical description of forward pp and $p\bar{p}$ scattering. Since their introduction [12] they were shown to be important for the analysis of forward scattering, determining structure and parameters of the real amplitude.

APPENDIX C: ALTERNATIVE SINGLE POLE POMERON APPROACH

In the $\log^2 s$ description of total cross section (high energies) the Pomeron intercept can be recovered when we take a convenient energy range of the total cross section in Eq. (18). Comparative analysis between the two main alternatives for the total cross section was performed [22] before the LHC era. In the present work we based our calculation of dispersion relations in the $\log^2 s$ approach (unitarized model). On the other hand in the $\log^2 s$ description of total cross section (high energies) the Pomeron intercept (single pole description) can be recovered when we take a convenient energy range of the total cross section. First we rewrite the dominant terms at high energies in the form

$$\sigma_{HE}(s) = P + H\log^2\left(\frac{s_0}{s_1}\right) - 4H\log\left(\frac{s_0}{s_1}\right)\log\left(\sqrt{\frac{s}{s_1}}\right)$$
$$+ 4H\log^2\left(\sqrt{\frac{s}{s_1}}\right), \tag{C1}$$

where we have introduced a new scale s_1 (in GeV^2) chosen appropriately in order to obtain the Pomeron intercept. After some algebra we can rewrite the above equation as

$$\sigma_{HE}(s) = P - H\log^2\left(\frac{s_0}{s_1}\right)$$
$$+ 2H\log^2\left(\frac{s_0}{s_1}\right)\left(1 + y + \frac{1}{2}y^2\right), \tag{C2}$$

where

$$y \equiv \log\left[\left(\frac{s}{s_1}\right)^{-1/\log\left(\frac{s_0}{s_1}\right)} \right]. \tag{C3}$$

For values $y \ll 1$, corresponding to $\sqrt{s} \ll 10^6$ GeV, we can exponentiate the terms in parentheses of Eq. (C2), writing

$$\sigma_{HE}(s) \simeq P - H\log^2\left(\frac{s_0}{s_1}\right) + 2H\log^2\left(\frac{s_0}{s_1}\right)e^{(y)}$$
$$= P + H\log^2\left(\frac{s_0}{s_1}\right)\left[2\left(\frac{s}{s_1}\right)^{\epsilon_0} - 1 \right], \tag{C4}$$

where

$$\epsilon_0 = -1/\log\left(\frac{s_0}{s_1}\right), \tag{C5}$$

which is the Pomeron intercept coefficient similar to the one in the Donnachie and Landshoff description. From the definition of ϵ_0 in terms of the scales, s_0 and s_1, we can rewrite Eq. (C4) as

$$\sigma_{HE}(s) \simeq P + \frac{H}{\epsilon_0}\left[2e^{-1}\left(\frac{s}{s_0}\right)^{\epsilon_0} - 1 \right]. \tag{C6}$$

Of course Eq. (C6) is compatible with Eq. (C2) only in a limited range of energy, and if one wants a better description of low energy data using Eq. (C2), the parameters P, H and also the parameters for the low energies R_1 and R_2, here not included explicitly, should be reobtained. The complete formula for total cross section in this powerlike representation is

$$\sigma^{\mp}(s) = P' + H'\left(\frac{s}{s_0}\right)^{\epsilon_0} + R_1'\left(\frac{s}{s_0}\right)^{-\eta_1'} \pm R_2'\left(\frac{s}{s_0}\right)^{-\eta_2'}, \tag{C7}$$

where we rewrite the parameter with prime in order to distinguish from Eq. (18). In Table V we give values for this

TABLE V. Suggested values for the parameters of the total cross section in the powerlike representation.

P' (mb)	H' (mb)	R_1' (mb)	R_2' (mb)	η_1'	η_2'	ϵ_0
−49.1	59.4	37.1	8.143	0.225	0.6144	0.059

representation. It is important to observe that the term P' in Eq. (C7) corresponds to a Regge trajectory with zero power coefficient.

Obviously this alternative representation can be written in terms of the variable x for use in dispersion relations.

[1] A. Donnachie, H. G. Dosch, P. V. Landshoff, and O. Nachtmann, *Pomeron Physics and QCD* (Cambridge University Press, Cambridge, England, 2002).

[2] A. Donnachie and P. V. Landshoff, Nucl. Phys. **231**, 189 (1984); Phys. Lett. B **296**, 227 (1992); Z. Phys. C **61**, 139 (1994).

[3] C. Bourrely, J. Soffer, and T. T. Wu, Phys. Rev. D **19**, 3249 (1979); Nucl. Phys. **B247**, 15 (1984); Eur. Phys. J. C **28**, 97 (2003); Int. J. Mod. Phys. A **30**, 1542006 (2015); C. Bourrely, J. M. Myers, J. Soffer, and T. T. Wu, Phys. Rev. D **85**, 096009 (2012); O. V. Selyugin, Phys. Rev. D **60**, 074028 (1999); Eur. Phys. J. C **72**, 2073 (2012); Phys. Rev. D **91**, 113003 (2015); V. A. Petrov, E. Predazzi, and A. V. Prokudin, Eur. Phys. J. C **28**, 525 (2003); E. Gotsman, E. Levin, and I. Potashnikova, Phys. Lett. B **781**, 155 (2018); Eur. Phys. J. C **77**, 632 (2017).

[4] N. Amos, Nucl. Phys. **B262**, 689 (1985); A. Breakstone, Nucl. Phys. **B248**, 253 (1994); C. Avila, Phys. Lett. B **445**, 419 (1999); C. Augier, Phys. Lett. B **344**, 451 (1995); F. Abe, Phys. Rev. D **50**, 5518 (1994).

[5] G. Antchev, Europhys. Lett. **101**, 21002 (2013); G. Aad, Nucl. Phys. **B889**, 486 (2014); M. Aaboud, Phys. Lett. B **761**, 158 (2016).

[6] H. G. Dosch, E. Ferreira, and A. Kramer, Phys. Rev. D **50**, 1992 (1994).

[7] A. K. Kohara, E. Ferreira, and T. Kodama, Phys. Rev. D **87**, 054024 (2013); Eur. Phys. J. C **73**, 2326 (2013); A. K. Kohara, E. Ferreira, and T. Kodama, Eur. Phys. J. C **74**, 3175 (2014).

[8] E. Gotsman, E. Levin, and U. Maor, Int. J. Mod. Phys. A **30**, 1542005 (2015).

[9] Y. Kovchegov and E. Levin, *Quantum Chromodynamics at High Energies* (Cambridge University Press, Cambridge, England, 2012).

[10] A. K. Kohara, E. Ferreira, T. Kodama, and M. Rangel, Eur. Phys. J. C **77**, 877 (2017).

[11] C. Bourrely, N. N. Khuri, A. Martin, J. Soffer, *Quarks, Gluons and Strong Interactions*, edited by Y. L. Dokshitzer, P. Levai, and J. Nyiri (World Scientific, 2006), pp. 125–128.

[12] E. Ferreira, Int. J. Mod. Phys. E **16**, 2893 (2007).

[13] C. Patrign *et al.* (Particle Data Group), Chin. Phys. C **40**, 100001 (2016).

[14] J. Sesma, E. Ferreira, and A. K. Kohara, Phys. Rev. C **97**, 014003 (2018); E. Ferreira, A. K. Kohara, and J. Sesma, J. Number Theory **172**, 21 (2017); E. Ferreira and J. Sesma, J. Math. Phys. (N.Y.) **49**, 033504 (2008); **54**, 033507 (2013).

[15] D. A. Fagundes, M. J. Menon and P. V. R. G. Silva, Int. J. Mod. Phys. A **32**, 1750184 (2017) (and references therein); R. F. Avila and M. J. Menon, Nucl. Phys. A **744**, 249 (2004); Braz. J. Phys. **37**, 358 (2007).

[16] H. Bethe, Ann. Phys. (N.Y.) **3**, 190 (1958); G. B. West and D. R. Yennie, Phys. Rev. **172**, 1413 (1968); R. Cahn, Z. Phys. C **15**, 253 (1982); V. Kundràt and M. Lokajcek, Phys. Lett. B **232**, 263 (1989); Mod. Phys. Lett. A **11**, 2241 (1996); V. A. Petrov, Eur. Phys. J. C **78**, 221 (2018).

[17] W. Brückner and B. Povh *et al.*, Z. Phys. A **339**, 367 (1991).

[18] C. Bourrely, A. Martin, J. Soffer, and D. Wray, J. Phys. G **3**, 295 (1977).

[19] M. L. Good and W. D. Walker, Phys. Rev. **120**, 1857 (1960).

[20] P. Jenni, P. Baillon, Y. Declais, M. Ferro-Luzzi, J. M. Perreau, J. Seguinot, and T. Ypsilantis, Nucl. Phys. **B129**, 232 (1977); H. Braun, J.-P. Gerber, G. Maurer, A. Michalon, B. Schiby, R. Strub, D. M. Chew, C. Ouannes, and Z. Strachman, Nucl. Phys. **B95**, 481 (1975); J. S. Russ *et al.*, Phys. Rev. D **15**, 3139 (1977); G. W. Brandenburg, R. K. Carnegie, R. J. Cashmore, M. Davier, D. W. G. S. Leith, J. Matthews, P. Walden, S. H. Williams, and F. Winkelmann, Phys. Lett. **58B**, 367 (1975); Yu. M. Antipov *et al.*, Nucl. Phys. **B57**, 333 (1973); Yu. M. Kazarinov *et al.*, Nucl. Phys. **B124**, 391 (1977); D. S. Ayres *et al.*, Phys. Rev. D **15**, 3105 (1977); B. V. Batyunia *et al.*, Yad. Fiz. **44**, 1489 (1986) [Sov. J. Nucl. Phys. **44**, 969 (1986)]; G. G. Beznogikh *et al.*, Nucl. Phys. **B54**, 78 (1973); A. A. Kuznetsov *et al.*, Yad. Fiz. **33**, 142 (1981) [Sov. J. Nucl. Phys. **33**, 74 (1981)]; D. Gross *et al.*, Phys. Rev. Lett. **41**, 1632 (1978); V. D. Apokin *et al.*, Yad. Fiz. **25**, 94 (1977) [Sov. J. Nucl. Phys. **25**, 51 (1977)]; N. Amos *et al.*, Nucl. Phys. **B262**, 689 (1985); R. E. Breedon *et al.*, Phys. Lett. B **216**, 459 (1989); UA6 Exp; CERN Libraries CM-P00051774; also R.E.B. Ph. D. thesis, Rockefeller University, 1988; C. W. Akerlof *et al.*, Phys. Rev. D **14**, 2864 (1976); Phys. Rev. Lett. **35**, 1406 (1975); L. A. Fajardo *et al.*, Phys. Rev. D **24**, 46 (1981); also L.A.F. Ph.D. thesis, Fermilab Library, 1980; A. Schiz *et al.*, Phys. Rev. D **24**, 26 (1981); I. Ambats, D. S. Ayres, R. Diebold, A. F. Greene, S. L. Kramer, A. Lesnik, D. R. Rust, C. E. W. Ward, A. B. Wicklund, and D. D. Yovanovitch, Phys. Rev. D **9**, 1179 (1974); J. P. Burq *et al.*, Nucl. Phys. **B217**, 285 (1983); Phys. Lett. **109B**, 124 (1982); M. Yu. Bogolyubsky *et al.*, Sov. J. Nucl. Phys. **41**, 773 (1989).

[21] A. Martin, Phys. Lett. B **404**, 137 (1997).

[22] J. R. Cudell, V. Ezhela, K. Kang, S. Lugovsky, and N. Tkachenko, Phys. Rev. D **61**, 034019 (2000).